Optoelectronic and Birefringence Properties of Weakly Mg Doped ZnO Thin lms Prepared By Spray Pyrolysis.

Yassine Bouachibaa
Laboratoire Technologie des Mat´eriaux Avanc´es
ABDELOUADOUD MAMMERI (abdelouadoud.mammeri@gmail.com)
Laboratoire Couches Minces et Interfaces, Universit´e de Fr´eres Mentouri Constantine 1
https://orcid.org/0000-0003-3820-3324
Abderrahmane Bouabellou
Laboratoire Couches Minces et Interfaces, Universit´e de Fr´eres Mentouri Constantine 1
Rabia Oualid
Laboratoire Technologie des Mat´eriaux Avanc´es
Saber Saidi
Laboratoire Technologie des Mat´eriaux Avanc´es
Adel Taabouche
Universit´e de Fr´eres Mentouri Constantine 1
Badis Rahal
Nuclear Techniques Division, Nuclear Research Center of Algiers
Lyes Benharrat
Research Center in Semiconductors Technology for Energy-CRTSE
Hacene Serrar
Research Center in Industrial Technologies (CRTI)
Moukhtar Boudissa
University Ferhat Abbas

Research Article

Keywords: Optoelectronic, birefringence, ZnO, pyrolysis

Posted Date: November 1st, 2021

DOI: https://doi.org/10.21203/rs.3.rs-1021475/v1

Optoelectronic and birefringence properties of weakly Mg doped ZnO thin films prepared by spray pyrolysis

Yassine Bouachiba[1], Abdelouadoud Mammeri[2*], Abderrahmane Bouabellou[2], Oualid Rabia[1], Saber Saidi[1], Adel Taabouche[2], Badis Rahal[3], Lyes Benharrat[4], Hacene Serrar[5] and Moukhtar Boudissa[6]

[1]Laboratoire Technologie des Matériaux Avancés,Ecole Nationale Polytechnique de Constantine Malek BENNABI,BP 75A RP,Ali Mendjeli, Constantine, Algérie.

[2*]Laboratoire Couches Minces et Interfaces, Université de Fréres Mentouri Constantine 1, Constantine, Algérie.

[3]Nuclear Techniques Division, Nuclear Research Center of Algiers, 2 Bd, Frantz Fanon, BP 399, 16000, Algiers, Algeria.

[4]Research Center in Semiconductors Technology for Energy-CRTSE, 02, Bd. Dr. Frantz Fanon, B.P. 140,7 Merveilles, 16038, Algiers, Algeria.

[5]Research Center in Industrial Technologies (CRTI), BP 64 Cheraga, Alger, Algeria.

[6]ENMC Laboratory, Department of Physics, Faculty of Science, University Ferhat Abbas, Setif, 19000, Algeria.

*Corresponding author(s). E-mail(s): abdelouadoud.mammeri@gmail.com;
Contributing authors: ybouachiba@gmail.com; a_bouabellou@yahoo.fr; oualidrabia28@gmail.com; saber18saidi@gmail.com; adelphm@gmail.com; b.rahal@crna.dz; benharrat.lyes@crtse.dz; serrarhacene@gmail.com; mokhtar.bousissa@univ-setif.dz;

1 Introduction

Zinc Oxide (ZnO) is is a multipurpose semiconductor with many uses such as ultra-capacitor electrode [1], spintronic devices [2], multigas sensing [3–6], piezoelectric devices [7], ultra-violet LEDs [8], detectors [9] as well as waveguides [10–12]. In its thin film form, ZnO has a large adaptation to several deposition methods such as chemical vapor deposition [13], pulsed laser deposition [14], spray pyrolysis [15], dip-coating [16] and electrochemical deposition [17]. ZnO has very interesting characteristics for application in electronics and optoelectronics devices, especially its exciton binding energy of 60 meV at 300K, a wide direct band gap of 3.37 eV [18]. In addition to an ordinary and extraordinary refractive indexes of $n_e = 2.006$ and $n_o = 1.990$ respectively [19]. To modify its electrical properties, ZnO was doped with Group III elements such as Al, Ga and In which acted as donor dopants to reinforce its n-type electrical nature and group V elements such as N, P, As and Sb which acted as acceptor dopants which changed ZnO to be a p-type semiconductor [20]. Controlling the refractive index of ZnO thin films was achieved by several ways including thermal annealing [21] and doping with In [22], Te, N [23] and Mg [24]. However, the effect of dopants on the optical and electrical properties of ZnO is still not well understood.

Tailoring ZnO optical and electrical properties via dopants while maintaining high quality films especially using spray pyrolysis is very attractive to both scientists and technology developers as it offers a control over several experimental parameters, it is cheap, uncomplicated and environmentally friendly.

Wurtzite $Mg_xZn_{1-x}O$ alloy is very interesting due to the high solubility of Mg in the ZnO wurtzite matrix (up to 30%) [25]. Moreover, it offers control over a range of optical and electrical properties of ZnO such as widening of the optical gap energy up to 0.85 eV [26], consequently, it can be used for multiple purposes such as a top layer in $Mg_xZn_{1-x}O$/ZnO multilayer UV photodetector [27] and high mobility MgZnO/ZnO thin film transistor [28] to name few. Concerning the waveguiding properties, little attention has been paid to wurtzite $Mg_xZn_{1-x}O$ as a waveguide, however, $Mg_xZn_{1-x}O$ was used as a buffer layer for ZnO waveguide thin film [29]. In an other work, a potential use of $Mg_xZn_{1-x}O$ cubic rocksalt-type phase as a wave guide was reported Yu et al. [30]. Wurtzite $Mg_xZn_{1-x}O$ thin film alloy refractive index was previously studied but there is still work to be done, as there are opposite results regarding the birefringence which is found to be negative in some studies [18, 31] and positive in another study[24].

In this work, we engaged in the investigation of the relations between the refractive index, the optical gap energy and the charge carriers' density in addition to the birefringence of $Mg_xZn_{1-x}O$ thin films deposited by spray pyrolysis on glass substrate.

2 Results and Discussion

2.1 XRD analysis

From Figure 1(a) we can see clearly that all films exhibit a crystalline hexagonal wurtzite structure (JCPDS card no. 00-036-1451) with the quasi-predominance of (002) peak indicating the preferential growth of undoped and Mg doped ZnO thin films through the c-axis direction. However, weak intensity peaks of other crystallographic directions were observed in the following positions 31.96°(100), 36.56°(101), 47.87°(102), 63.17°(103) and 72.85°(004). The peak (002) experienced a shift towards higher angles over Mg doping (Figure 1(b)) which was reported by a number of authors [32–34] and it is due to the difference in the ionic radius between Mg^{+2} (0.57 Å) and Zn^{+2} (0.60 Å) [35]. This difference is directly related to the compression strain on the main axes of the wurtzite structure a and c. Previously, Chang et al. [36] reported also similar compression strain in their sputtered MgZnO thin films which were interpreted by good substitution between Mg and Zn ions.
The grain size can be calculated by Debye-Scherrer formula [32]:

$$D = \frac{K\lambda}{\beta \cos(\theta)} \tag{1}$$

where λ is the wavelength of the incident X-ray, θ is the Bragg's angle, K is the shape factor (0.9 for gaussian fit) and β is the Full Width at Half Maxima (FWHM) of the peaks. The crystallite size, lattice parameters and strain axes are tabulated in table 1. It should be noted that there was no significant change in the average crystallite size (33.13 nm for Mg_0Zn_1O film and an average of 33.03 nm for the $Mg_xZn_{1-x}O$ films) and the minus sign of the strain values (ϵ_a and ϵ_c) approves the compression nature of the strain. To calculate lattice parameter c of the thin films we used the Bragg's law (with n=1) and the d spacing of wurtzite structure.

2.2 UV-Vis measurements

The transmittance of the thin films was slightly enhanced on average with the introduction of Mg in the visible region (400-800 nm). The limit of the absorption zone was shifted to smaller wavelengths which renders the thin films to be more dielectric as Mg doping is increased, this effect is directly related to the blue shift of the optical band gap and it was approximated for each film using the Tauc's plot:

$$\alpha h\nu = A(h\nu - E_g)^n \tag{2}$$

where $h\nu$ is the photon energy, E_g is the optical gap energy, A is constant and n equals $\frac{1}{2}$ since ZnO has a direct band gap. The widening of the optical band gap could be ascribed to the difference in electronegativity between Zn^{+2} and Mg^{+2} ions [37–39]. In similar study, Al-Ghamdi [40] reported this correlation

between the optical band gap energy and the electronegativity in his work about amorphous $Se_{96-x}Te_4Ag_x$ thin films.
In fact, it should be noted that both the electronegativity and electron affinity are directly related [41]. In this way Figure 4 presents the calculated optical band gap and the electron affinity versus Mg doping. The electron affinity ($e\chi$) was quantitatively calculated using Vegard's law [42]:

$$e\chi(Mg_xZn_{1-x}O) = e\chi(ZnO) - (e\chi(ZnO) - e\chi(MgO))x \quad (3)$$

$e\chi(ZnO)$, $e\chi(MgO)$ have the value of 4.5 eV [43] and 0.85 eV [44] for the electron affinity of ZnO and MgO respectively. Previously, iskenderoglu et al. [25] approved experimentally by UPS technique the inverse relation between the optical gap energy and the electron affinity of sprayed MgZnO alloy thin film, with Mg doping ranging from 0 to 15%.

2.3 Photoluminescence

The room temperature photoluminescence spectra are shown in Figure 5. The undoped thin film had four peaks at 381 (3.25 eV), 416 (2.98 eV), 441 (2.81 eV) and 505 nm (2.46 eV) which were explained by: the emission corresponding to excitons recombination, zinc interstitial (Zn_i), oxygen vacancies (V_O) and donor V_O – acceptor V_{Zn} recombination respectively [45, 46]. The same peaks were observed also in $Mg_{0.01}Zn_{0.99}O$ except a blue shift of the 380 peak to 381 nm (3.26 eV). The $Mg_{0.03}Zn_{0.97}O$ thin film had three peaks 379 (3.27 eV), 416 (2.81 eV) and 492 nm (2.52 eV) and they were attributed to excitons recombination, zinc interstitial (Zn_i) [45] and oxygen vacancy (V_O) [47] respectively. Finally the $Mg_{0.05}Zn_{0.95}O$ thin film exhibited two peaks at 378 (3.28 eV) and 503 nm (2.47 eV) and they were manifestations of excitons and donor V_O – acceptor V_{Zn} recombinations [45, 46]. The blue shift of the near band edge emission from the PL peaks was in consistency with the UV visible calculations of the optical band gap, however, it was at a lower rate which was explained by stokes shift [48].

2.4 Electrical measurements

Figure 6 demonstrates the near isotropic electric transportation of the deposited films which could be attributed to the fact that the films have the predominant orientation (002) of the wurtzite structure [49].
The free charge carriers' density decreased from 3.146×10^{18} for the undoped film to 9.273×10^{13} cm^{-3} for $Mg_{0.05}Zn_{0.95}O$ film. In parallel, the resistivity increased from 109 to 1268 Ω cm and the mobility increased from 0.01821 to 53.08 $cm^2/(V.s)$. The decreased charge carriers' density could be attributed to the fact that the conduction band (CB) of pure ZnO consists mainly of O_{2p} and Zn_{4s} states [50, 51], so the introduction of Mg in ZnO thin films will reduce the Zn_{4s} state and introduce Mg_{3p} state which has high energy relative to the Zn_{4s} [52, 53]. Moreover, the widening in the optical bang gap energy

discussed previously, could also influence the free charge carriers' density since the electrons passing from the valance band must requires higher energy to access the conduction band.

2.5 Surface morphology

Figure 8 shows the morphology of undoped and 5 at. % doped ZnO thin films. The undoped (Figure 8(a)) thin film shows a dense surface with granular mixture of small grains and large aggregates. The size of the small grains varies from $\sim$ 20 to 80 nm and that of the aggregates reaches $\sim$ 200-300 nm. From the doped sample (Figure 8(b)), it is evident that magnesium has a tendency to promote the phenomenon of coalescence. This doped film shows a less dense and relatively homogeneous morphology with large aggregates whose size varies from $\sim$ 200 to 500 nm.
No cracks nor empty holes were observed on the surface of the films, revealing the high quality of our films.

2.6 M-lines measurements

The M-lines measurements demonstrated the guiding modes present in the films. All films had four guiding modes (TE_0, TE_1, TM_0, and TM_1) two for each optical polarization (Transverse Electric mode (TE) and Transverse Magnetic mode (TM)) as illustrated in Figure 9. Using the dispersion equations for TE and TM polarizations, the optogeometric parameters can be calculated [54–56]. The effective indices, the films thicknesses and the birefringence values are presented in Table 2.
Figure 10 illustrate the variation of n_{TE}, n_{TM}, optical gap energy and free charge carriers' density as a function of the Mg concentration. The slight difference between n_{TM} and n_{TE} confirmed the birefringence behavior of our films. This made the guided waves traveling during the TE mode in the plane perpendicular to the *c*-axis of the wurtzite structure submit to an ordinary refractive index (n_{TE}) and during the TM mode to an extraordinary one (n_{TM}) [19]. Both n_{TE} and n_{TM} were found to decreased over Mg doping. This behavior seems to be in good agreement with the broadening of the optical band gap and the depletion of the conduction band free charge carriers' (Figure 10) [57]. The birefringence was measured to be positive for all films which is a good indication for the unchanging orientations of the bonds Zn-O with the replacement of Zn by Mg [58, 59].
The inverse relation between the optical gap energy, the resistivity and the refractive index as Mg content increased in the ZnO thin film was also observed by Kaushal et al. [60]. The same fact has been reported by Teng et al. [24] for Mg-doped ZnO thin films prepared by pulsed laser deposition. In similar study, Sorar et al. [61] found that the ordinary refractive index generally decreases with the increase of the Si doping in ZnO thin films prepared by sol-gel and annealed at 350 °C and 550 °C whereas their optical band gap energy was found to be blue shifted.

3 Tables

4 Figures

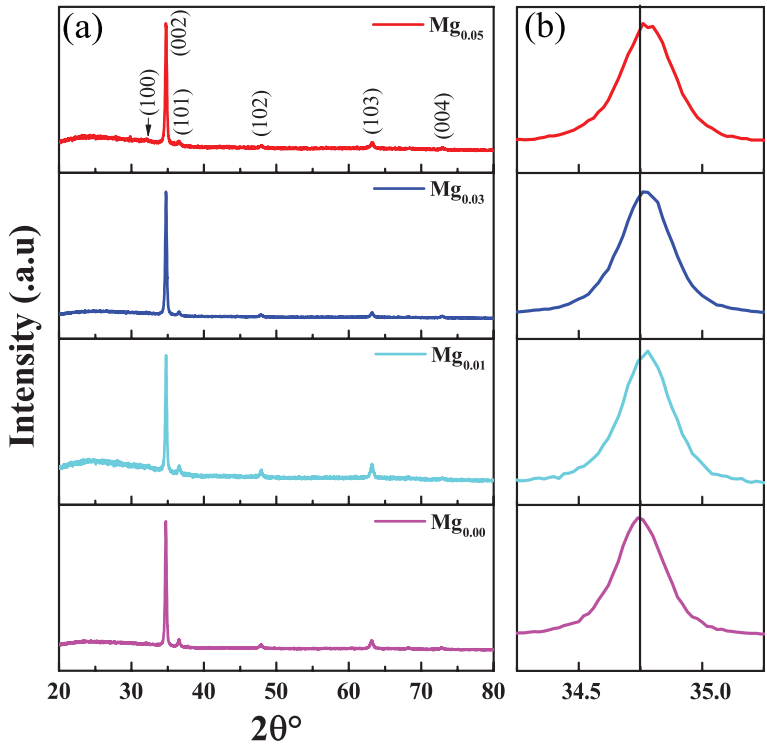

Fig. 1 (a) XRD spectra of undoped and Mg doped ZnO thin films, (b) an emphasis of the (002) peak showing a shift towards higher angles for the doped thin films.

5 Methods

The sprayed solution for the undoped ZnO thin films was prepared by dissolving the proper amount of dihydrate zinc acetate [$Zn(CH_3CO_2)_2 \cdot 2H_2O$] in 99.98% pure methanol to obtain 0.1 M solution that was submitted to a constant stirring at 60 °C for 45 min on a magnetic stirrer. Concerning the sprayed solution of the Mg doped ZnO thin films, we maintained the same parameters with the use of magnesium chloride [$Mg(CH_3CO_2)_2 \cdot 4H_2O$] as Mg precursor and each time the proper amount was added to 0.1 M methanol solutions of $Zn(CH_3CO_2)_2 \cdot 2H_2O$ to produce the following contents of zinc and magnesium: $Mg_xZn_{1-x}O$ with x equals 0.01, 0.03 and 0.05.

An ordinary glass substrate were ultra-sonically cleaned in a 1:1 mixture of acetone and ethanol for 15 min and left to dry in air. The films were deposited

Table 1 The information obtained and calculated from the XRD spectra.

Sample	2θ (degree)	d spacing (Å)	Crystallite size (nm)	a(Å)	c(Å)	ϵ_a (10^{-3})	ϵ_c (10^{-3})
$Mg_{0.00}Zn_{1.00}O$	34.75	2.580	33.13	3.2306	5.1592	-3.4241	-5.4746
$Mg_{0.01}Zn_{0.99}O$	34.77	2.455	31.26	3.2240	5.1560	-5.4601	-6.0915
$Mg_{0.03}Zn_{0.97}O$	34.77	2.456	31.30	3.2256	5.1560	-4.9665	-6.0915
$Mg_{0.05}Zn_{0.95}O$	34.78	2.577	35.83	3.2298	5.1547	-3.6709	-6.3421

Table 2 Optogeometric Properties of the deposited thin films.

Sample	Effective index $\pm 10^{-4}$				Refractive index 10^{-4}		Thickness TE	Thickness TM	Birefringence
	TE_0	TE_1	TM_0	TM_1	n_{TE}	n_{TM}	$\pm 0.1nm$	$\pm 0.1nm$	$(n_{TM} - n_{TE})$
$Mg_{0.00}Zn_1.00O$	1.8923	1.6565	1.8793	1.6033	1.9699	1.9761	436.1	452.1	0.0062
$Mg_{0.01}Zn_{0.99}O$	1.8758	1.5994	1.8539	1.5486	1.9680	1.9682	347.4	382.6	0.0002
$Mg_{0.03}Zn_{0.97}O$	1.8738	1.6203	1.8581	1.5647	1.9580	1.9652	413.1	426.3	0.0072
$Mg_{0.05}Zn_{0.95}O$	1.8451	1.5981	1.8278	1.5494	1.9278	1.9314	417.7	433.7	0.0036

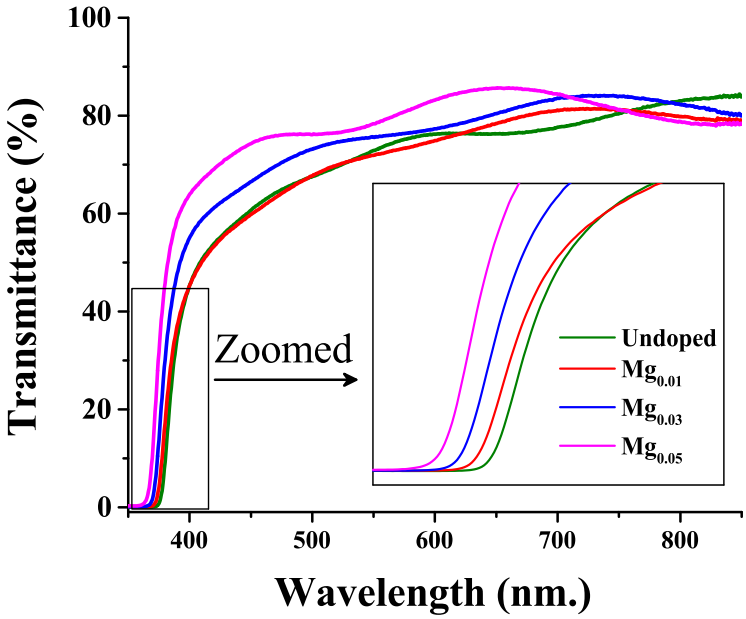

Fig. 2 Transmittance spectra of pure and doped ZnO thin films zoomed in the absorption region.

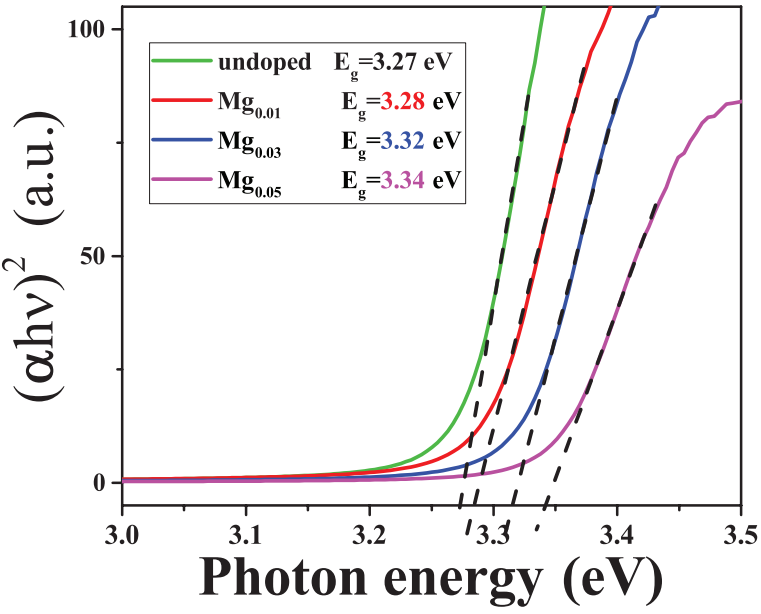

Fig. 3 Tauc's plot for the undoped and doped ZnO thin films.

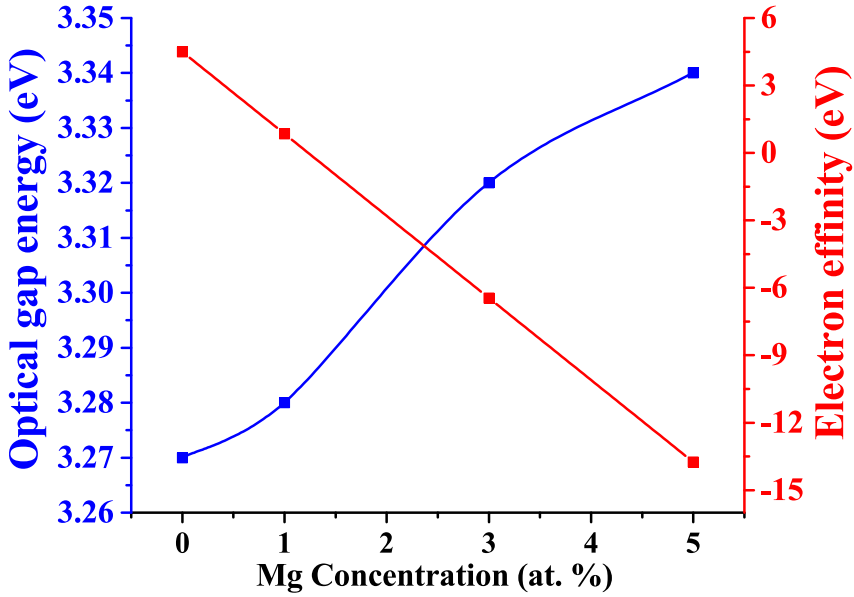

Fig. 4 The evolution of the optical band gap energy and the electron affinity of $Mg_xZn_{1-x}O$ thin films as a function of Mg concentration.

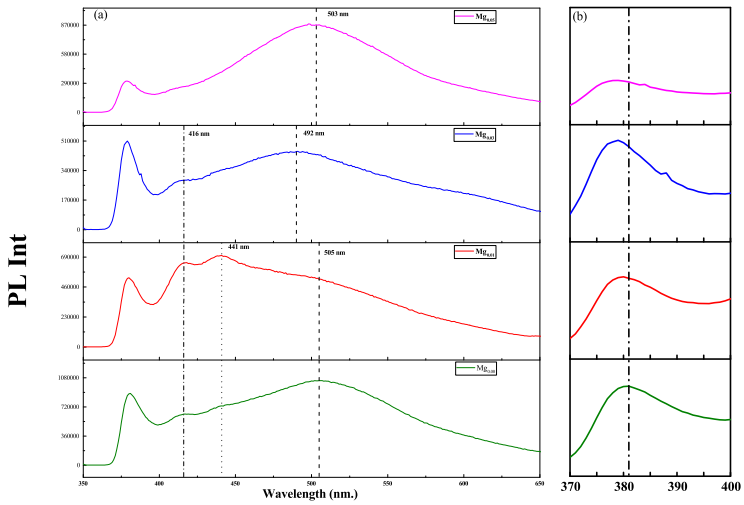

Fig. 5 (a) Room temperature photoluminescence spectra, (b) an emphasis of the excitons recombination peaks.

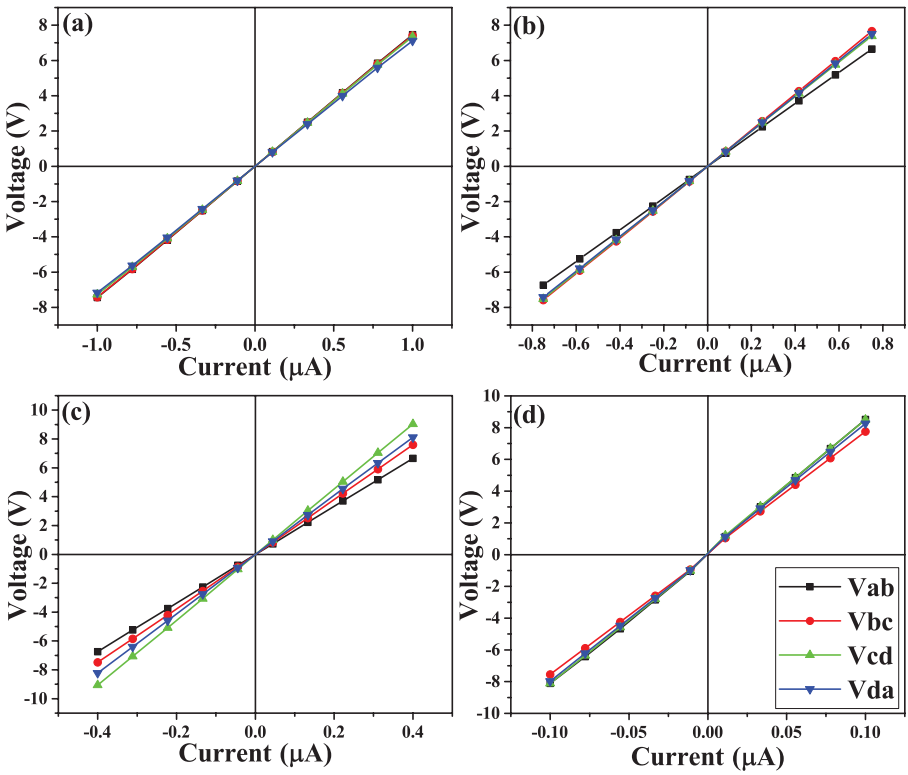

Fig. 6 I-V measurements for the four thin films: (a) undoped ZnO, (b) $Mg_{0.01}Zn_{0.99}O$, (c) $Mg_{0.03}Zn_{0.97}O$ and (d) $Mg_{0.05}Zn_{0.95}O$.

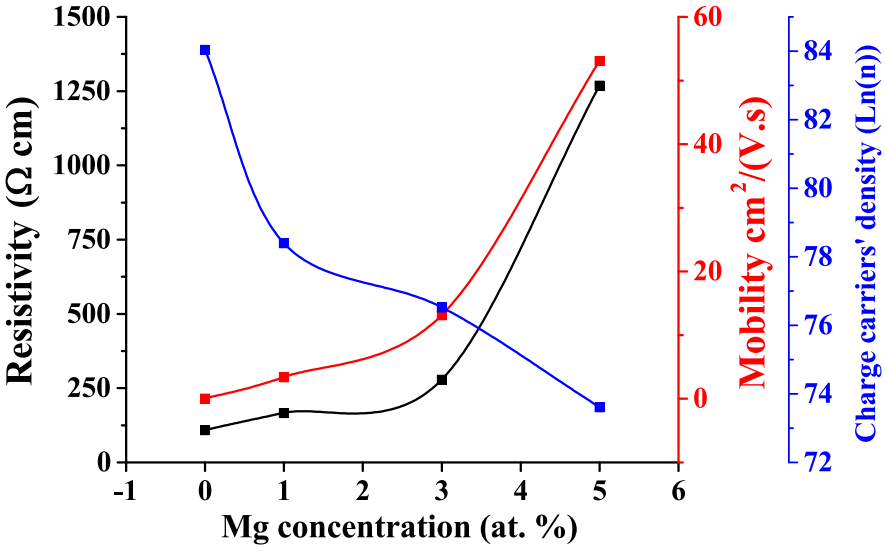

Fig. 7 Resistivity (ρ) and charge carriers (n) as a function of Mg concentration.

using spray pyrolysis system. The deposition temperature was 450 °C.
In order to characterize our thin films, multiple techniques were used: Philips PANalytical X'Pert Pro diffractometer with a wave length of 1.5406 Å, environmental scanning electron microscope Philips XL30 ESEM FEG and for the electrical properties Ecopia HMS-3000 hall effect measurement system, finally for the optical measurements, Metricon 2010/M Prism (rutile TiO_2: n_e=2,8639 and n_o=2.5822 at 632,8 nm with an apical angle of 44,60 °) Coupler was used to couple 632.8 nm HeNe laser light into air/$Mg_xZn_{1-x}O$/glass waveguide and Shimadzu UV-3101PC Spectrophotometer.

6 Conclusion

Mg doped ZnO thin films were successfully deposited on glass substrate via spray pyrolysis at 450 °C. The XRD characterization showed highly *c* oriented thin films with a decrease in *a* and *c* as the Mg concentration increased in the thin films. The undoped thin film had a multisize grain distribution meanwhile the $Mg_{0.05}Zn_{0.95}O$ had a more homogeneous grain distribution. Mg doping in the ZnO films led to a blue shift of the optical band gap energy and a depletion of the conduction band due to the drop in free carriers' density that had a direct effect on the ordinary and the extraordinary refractive indexes that were found to decrease. The birefringence of a crystal depends on multiple factors such as strain, defects charge carriers' density, bounds orientations and so on, therefore it will change from papers to papers with the change of deposition method especially.

Declarations

- Funding: Not applicable
- Conflict of interest/Competing interests: The authors declare that they have no conflict of interest.
- Ethics approval: Not applicable
- Consent to participate: Not applicable
- Consent for publication: Not applicable
- Availability of data and materials: Not applicable
- Code availability: Not applicable
- Authors' contributions: Not applicable

References

[1] Lakshmi, K., Revathi, S.: Rice-like zno architecture: An eminent electrode material for high-performance ultracapacitor application. Journal of Inorganic and Organometallic Polymers and Materials **31**(5), 1992–2002 (2021). https://doi.org/10.1007/s10904-021-01922-5

[2] Pearton, S., Norton, D., Heo, Y., Tien, L.-C., Ivill, M., Li, Y., Kang, B., Ren, F., Kelly, J., Hebard, A.: Zno spintronics and nanowire devices.

Journal of Electronic Materials **35**, 862–868 (2006). https://doi.org/10.1007/BF02692541

[3] Hosseinnejad, M.T., Shirazi, M., Ghoranneviss, M., Hantehzadeh, M.R., Darabi, E.: Preparation of nanostructured zno thin films using magnetron sputtering for the gas sensors applications. Journal of Inorganic and Organometallic Polymers and Materials **26**(2), 405–412 (2016). https://doi.org/10.1007/s10904-015-0324-0

[4] Hjiri, M., Bahanan, F., Aida, M., El Mir, L., Neri, G.: High performance co gas sensor based on zno nanoparticles. Journal of Inorganic and Organometallic Polymers and Materials **30**(10), 4063–4071 (2020). https://doi.org/10.1007/s10904-020-01553-2

[5] Blauw, M., Dam, V.A., Crego-Calama, M., Brongersma, S., Musschoot, J., Detavernier, C.: Oxygen sensing with zno thin films. Proceedings of IEEE Sensors **28–31**, 1416–1419 (2011). https://doi.org/10.1109/ICSENS.2011.6127128

[6] Patil, V.L., Vanalakar, S.A., Patil, P.S., Kim, J.H.: Fabrication of nanostructured zno thin films based no2 gas sensor via silar technique. Sensors and Actuators B: Chemical **239**, 1185–1193 (2017). https://doi.org/10.1016/j.snb.2016.08.130

[7] Polewczyk, V., Maffei, R., Vinai, G., Cicero, M., Prato, S., Capaldo, P., Zilio, S., Bona, A., Paolicelli, G., Mescola, A., D'Addato, S., Torelli, P., Benedetti, S.: Zno thin films growth optimization for piezoelectric application. Sensors **21**, 6114 (2021). https://doi.org/10.3390/s21186114

[8] Sandeep, K.M., Bhat, S., Dharmaprakash, S.M.: Structural, optical, and led characteristics of zno and al doped zno thin films. Journal of Physics and Chemistry of Solids **104**, 36–44 (2017). https://doi.org/10.1016/j.jpcs.2017.01.003

[9] Shaikh, S., Ganbavle, V., Inamdar, S., Rajpure, K.: Multifunctional zinc oxide thin films for high performance uv photodetector and nitrogen dioxide gas sensor. RSC Adv. **6** (2016). https://doi.org/10.1039/C6RA01750A

[10] Kamauchi, M., Shiosaki, T., Kawabata, A.: Channel optical waveguides of zno thin films. In: [Proceedings] 1990 IEEE 7th International Symposium on Applications of Ferroelectrics, pp. 733–736 (1990). https://doi.org/10.1109/ISAF.1990.200361

[11] Yu, S.F., Yuen, C., Lau, S.P., Fan, W.J.: Design and fabrication of zinc oxide thin-film ridge waveguides on silicon substrate with ultraviolet amplified spontaneous emission. IEEE Journal of Quantum Electronics

40(4), 406–412 (2004). https://doi.org/10.1109/JQE.2004.825212

[12] Teraoka, E., Kita, T., Tsukazaki, A., Kawasaki, M., Yamada, H.: Fabrication of zno channel waveguides for nonlinear optical applications. Proceedings of SPIE - The International Society for Optical Engineering **7940** (2011). https://doi.org/10.1117/12.874439

[13] Chen, Z., Shum, K., Salagaj, T., Zhang, W., Strobl, K.: Zno thin films synthesized by chemical vapor deposition, pp. 1–6 (2010). https://doi.org/10.1109/LISAT.2010.5478331

[14] Shan, F.K., Shin, B.C., Jang, S.W., Yu, Y.S.: Substrate effects of zno thin films prepared by pld technique. Journal of the European Ceramic Society **24**(6), 1015–1018 (2004). https://doi.org/10.1016/S0955-2219(03)00397-2. Electroceramics VIII

[15] Lehraki, N., Aida, M.S., Abed, S., Attaf, N., Attaf, A., Poulain, M.: Zno thin films deposition by spray pyrolysis: Influence of precursor solution properties. Current Applied Physics **12**(5), 1283–1287 (2012). https://doi.org/10.1016/j.cap.2012.03.012

[16] Rahal, B., Boudine, B., Larbah, Y., Siad, M., Souami, N.: Influence of low cd-doping concentration (0.5 and 3 wt.%) and different substrate types (glass and silicon) on the properties of dip-coated nanostructured zno semiconductors thin films. Journal of Inorganic and Organometallic Polymers and Materials, 1–17 (2021). https://doi.org/10.1007/s10904-021-02024-y

[17] Hamidi, A.S., Abidin, M.S.Z.: Electrochemical deposition of zinc oxide thin film using two-terminal setup. In: 2017 IEEE Regional Symposium on Micro and Nanoelectronics (RSM), pp. 34–37 (2017). https://doi.org/10.1109/RSM.2017.8069136

[18] Ellmer, K., Klein, A., Rech, B. (eds.): Transparent Conductive Zinc Oxide: Basics and Applications in Thin Film Solar Cells. Springer series in materials science, vol. 104. Springer, Berlin (2008). OCLC: ocn181423059

[19] Mehan, N., Tomar, M., Gupta, V., Mansingh, A.: Optical waveguiding and birefringence properties of sputtered zinc oxide (zno) thin films on glass. Optical Materials **27**(2), 241–248 (2004). https://doi.org/10.1016/j.optmat.2004.03.005

[20] Jagadish, C., Pearton, S.J.: Zinc Oxide Bulk, Thin Films and Nanostructures: Processing, Properties, and Applications vol. 7. Elsevier, ??? (2011)

[21] Huang, B., Li, J., Wu, Y.-b., Guo, D.-h., Wu, S.-t.: Optical constants of

transparent zno films by rf magnetron sputtering. Materials Letters **62**(8), 1316–1318 (2008). https://doi.org/10.1016/j.matlet.2007.08.043

[22] Xie, G.C., Fanga, L., Peng, L.P., Liu, G.B., Ruan, H.B., Wu, F., Kong, C.Y.: Effect of In-doping on the Optical Constants of ZnO Thin Films. Physics Procedia **32**, 651–657 (2012). https://doi.org/10.1016/j.phpro.2012.03.614. Accessed 2021-07-23

[23] Cai, A.L., Muth, J.F., Porter, H.L., Kvit, A., Narayan, J.: The refractive index and other properties of doped zno films. MRS Proceedings **764**, 3–21 (2003). https://doi.org/10.1557/PROC-764-C3.21

[24] Teng, C., Muth, J., Ozgur, U., Bergmann, M., Everitt, H., Sharma, A., Jin, C., Narayan, J.: Refractive indices and absorption coefficients of mgxzn1-xo alloys. Applied Physics Letters **76**, 979–981 (2000). https://doi.org/10.1063/1.125912

[25] iskenderoglu, D., Kasapoglu, A., Gür, E.: Valance band properties of mgzno thin films with increasing mg content; phase separation effects. Materials Research Express **6** (2018). https://doi.org/10.1088/2053-1591/aaf45e

[26] Özgür, ., Alivov, Y.I., Liu, C., Teke, A., Reshchikov, M.A., Doğan, S., Avrutin, V., Cho, S.-J., Morkoç, H.: A comprehensive review of zno materials and devices. Journal of Applied Physics **98**(4), 041301 (2005) https://arxiv.org/abs/https://doi.org/10.1063/1.1992666. https://doi.org/10.1063/1.1992666

[27] Rana, V.S., Rajput, J.K., Pathak, T.K., Purohit, L.P.: Multilayer mgzno/zno thin films for uv photodetectors. Journal of Alloys and Compounds **764**, 724–729 (2018). https://doi.org/10.1016/j.jallcom.2018.06.139

[28] Yue, D., Guo, S., Han, S., Cao, P., Zeng, Y., Xu, W., Fang, M., Liu, W., Zhu, D., Lu, Y., Qian, Y.: Facile fabrication of mgzno/zno composites for high performance thin film transistor. Journal of Alloys and Compounds **873**, 159840 (2021). https://doi.org/10.1016/j.jallcom.2021.159840

[29] Jia, C.-L., Wang, K.-M., Wang, X.-L., Zhang, X.-J., Lu, F.: Formation of c-axis oriented zno optical waveguides by radio-frequency magnetron sputtering. Optics express **13**, 5093–9 (2005). https://doi.org/10.1364/OPEX.13.005093

[30] Yu, P., Wu, H.Z., Xu, T.N., Qiu, D.J., Hu, G.J., Dai, N.: Cubic phase mgxzn1-xo thin films for optical waveguides. Journal of Crystal Growth **310**(2), 336–340 (2008). https://doi.org/10.1016/j.jcrysgro.2007.10.028

[31] Morkoç, H., Özgür, m.: Zinc Oxide: Fundamentals, Materials and Device Technology, 1st edn. Wiley, ??? (2009). https://doi.org/10.1002/9783527623945. https://onlinelibrary.wiley.com/doi/book/10.1002/9783527623945 Accessed 2021-07-26

[32] Khorramshahi, V., Karamdel, J., Yousefi, R.: Acetic acid sensing of Mg-doped ZnO thin films fabricated by the sol–gel method. Journal of Materials Science: Materials in Electronics **29**(17), 14679–14688 (2018). https://doi.org/10.1007/s10854-018-9604-0. Accessed 2021-06-18

[33] Kim, T.H., Park, J.J., Nam, S.H., Park, H.S., Cheong, N.R., Song, J.K., Park, S.M.: Fabrication of Mg-doped ZnO thin films by laser ablation of Zn:Mg target. Applied Surface Science **255**(10), 5264–5266 (2009). https://doi.org/10.1016/j.apsusc.2008.07.105. Accessed 2021-06-18

[34] Shan, F.K., Kim, B.I., Liu, G.X., Liu, Z.F., Sohn, J.Y., Lee, W.J., Shin, B.C., Yu, Y.S.: Blueshift of near band edge emission in Mg doped ZnO thin films and aging. Journal of Applied Physics **95**(9), 4772–4776 (2004). https://doi.org/10.1063/1.1690091. Accessed 2021-06-18

[35] Rouchdi, M., Salmani, E., Fares, B., Hassanain, N., Mzerd, A.: Synthesis and characteristics of Mg doped ZnO thin films: Experimental and ab-initio study. Results in Physics **7**, 620–627 (2017). https://doi.org/10.1016/j.rinp.2017.01.023. Accessed 2021-06-18

[36] Chang, R.-C., Chu, S.-Y., Yeh, P.-W., Hong, C.-S., Kao, P.-C., Huang, Y.-J.: The influence of Mg doped ZnO thin films on the properties of Love wave sensors. Sensors and Actuators B: Chemical **132**(1), 290–295 (2008). https://doi.org/10.1016/j.snb.2008.01.038. Accessed 2021-06-18

[37] Hussain, F., Imran, M., Khalil, R.M.A., Niaz, N.A., Rana, A.M., Sattar, M.A., Ismail, M., Majid, A., Kim, S., Iqbal, F., Javid, M.A., Saeed, S., Sattar, A.: An insight of Mg doped ZnO thin films: A comparative experimental and first-principle investigations. Physica E: Low-dimensional Systems and Nanostructures **115**, 113658 (2020). https://doi.org/10.1016/j.physe.2019.113658. Accessed 2021-06-18

[38] Huang, K., Tang, Z., Zhang, L., Yu, J., Lv, J., Liu, X., Liu, F.: Preparation and characterization of Mg-doped ZnO thin films by sol–gel method. Applied Surface Science **258**(8), 3710–3713 (2012). https://doi.org/10.1016/j.apsusc.2011.12.011. Accessed 2021-06-18

[39] Agrawal, A., Dar, T.A., Sen, P., Phase, D.M.: Transport and magneto-transport study of Mg doped ZnO thin films. Journal of Applied Physics **115**(14), 143701 (2014). https://doi.org/10.1063/1.4870864. Accessed 2021-06-18

[40] Al-Ghamdi, A.A.: Optical band gap and optical constants in amorphous Se96-xTe4Agx thin films. Vacuum **80**(5), 400–405 (2006). https://doi.org/10.1016/j.vacuum.2005.07.003. Accessed 2021-09-18

[41] Mulliken, R.S.: A New Electroaffinity Scale; Together with Data on Valence States and on Valence Ionization Potentials and Electron Affinities. The Journal of Chemical Physics **2**(11), 782–793 (1934). https://doi.org/10.1063/1.1749394. Accessed 2021-09-17

[42] Vegard, L.: Die konstitution der mischkristalle und die raumfüllung der atome. Zeitschrift für Physik **5**(1), 17–26 (1921)

[43] Hussain, B., Aslam, A., Khan, T.M., Creighton, M., Zohuri, B.: Electron affinity and bandgap optimization of zinc oxide for improved performance of zno/si heterojunction solar cell using pc1d simulations. Electronics **8**(2), 238 (2019)

[44] Aboelfotoh, M.O., Lorenzen, J.A.: Influence of secondary-electron emission from mgo surfaces on voltage-breakdown curves in penning mixtures for insulated-electrode discharges. Journal of Applied Physics **48**(11), 4754–4759 (1977) https://arxiv.org/abs/https://doi.org/10.1063/1.323490. https://doi.org/10.1063/1.323490

[45] Mishra, S., Srivastava, R., Prakash, S., Yadav, R., Panday, A.: Photoluminescence and photoconductive characteristics of hydrothermally synthesized zno nanoparticles. Opto-Electronics Review **18**(4), 467–473 (2010)

[46] Chen, H., Ding, J., Guo, W., Chen, G., Ma, S.: Blue-green emission mechanism and spectral shift of al-doped zno films related to defect levels. RSC Adv. **3**, 12327–12333 (2013). https://doi.org/10.1039/C3RA40750K

[47] Babu, K.S., Reddy, A.R., Sujatha, C., Reddy, K.V., Mallika, A.: Synthesis and optical characterization of porous zno. Journal of Advanced Ceramics **2**(3), 260–265 (2013)

[48] Kim, T.H., Park, J.J., Nam, S.H., Park, H.S., Cheong, N.R., Song, J.K., Park, S.M.: Fabrication of mg-doped zno thin films by laser ablation of zn: Mg target. Applied Surface Science **255**(10), 5264–5266 (2009)

[49] Oliveira, M., Castro, A., Marques, M., Rubio, A.: On the use of neumann's principle for the calculation of the polarizability tensor of nanostructures. Journal of nanoscience and nanotechnology **8**, 3392–8 (2008). https://doi.org/10.1166/jnn.2008.142

[50] Hu, Y., Zeng, H., Du, J., Hu, Z., Zhang, S.: The structural, electrical and optical properties of mg-doped ZnO with different interstitial mg

concentration. Materials Chemistry and Physics **182**, 15–21 (2016). https://doi.org/10.1016/j.matchemphys.2016.05.065. Accessed 2021-06-29

[51] Bustanafruz, F., Fazli, M., Mohammadizadeh, M.R., Jafar Tafreshi, M.: Optical and electronic properties of h-doped ZnO. Optical and Quantum Electronics **48**(5), 297 (2016). https://doi.org/10.1007/s11082-016-0575-1. Accessed 2021-06-29

[52] Wang, J., Tu, Y., Yang, L., Tolner, H.: Theoretical investigation of the electronic structure and optical properties of zinc-doped magnesium oxide. Journal of Computational Electronics **15**, 1521–1530 (2016). https://doi.org/10.1007/s10825-016-0906-2

[53] Zheng, W., Feng, Z.C., Chang, F.H., Lee, J.F., Zheng, R.S., Wuu, D.S., Liu, C.W.: Study of $Mg_xZn_{1-x}O$ Alloys ($0<x<0.15$) by X-Ray Absorption Spectroscopy. Advanced Materials Research **663**, 361–365 (2013). https://doi.org/10.4028/www.scientific.net/AMR.663.361. Accessed 2021-07-29

[54] Bouachiba, Y., Taabouche, A., Bouabellou, A., Hanini, F., Sedrati, C., Merabti, H.: Tio waveguides thin films prepared by sol-gel method on glass substrates with and without zno underlayer. Materials Science-Poland **38**(3), 381–385 (2020). https://doi.org/10.2478/msp-2020-0043

[55] Medjaldi, F., Bouabellou, A., Bouachiba, Y., Taabouche, A., Bouatia, K., Serrar, H.: Study of TiO2, SnO2 and nanocomposites TiO2:SnO2 thin films prepared by sol-gel method: Successful elaboration of variable–refractive index systems **7**(1), 016439 (2020). https://doi.org/10.1088/2053-1591/ab6c0c

[56] Gharbi, B., Taabouche, A., Brella, M., Gheriani, R., Bouachiba, Y., Bouabellou, A., Hanini, F., Barouk, S.L., Serrar, H., Rahal, B.: Spray pyrolysis synthesized and zno–nio nanostructured thin films analysis with their nanocomposites for waveguiding applications. Semiconductors **55**, 37–43 (2021)

[57] Feynman, R.P., Leighton, R.B., Sands, M.: The Feynman Lectures on Physics; New Millennium Ed. Basic Books, New York, NY (2010). Originally published 1963-1965. https://cds.cern.ch/record/1494701

[58] Weber, H.-J.: Anisotropic bond polarizabilities in birefringent crystals. Acta Crystallographica Section A **44**(3), 320–326 (1988). https://doi.org/10.1107/S0108767387012492

[59] Lidin, S.: Mapping bond orientations with polarized x-rays. Science **344**(6187), 969–970 (2014). https://doi.org/10.1126/science.1254902

[60] Kaushal, A., Kaur, D.: Effect of mg content on structural, electrical and

optical properties of zn1-xmgxo nanocomposite thin films. Solar Energy Materials and Solar Cells **93**, 193–198 (2009). https://doi.org/10.1016/j.solmat.2008.09.039

[61] Sorar, I., Saygin-Hinczewski, D., Hinczewski, M., Tepehan, F.Z.: Optical and structural properties of si-doped zno thin films. Applied Surface Science **257**(16), 7343–7349 (2011). https://doi.org/10.1016/j.apsusc.2011.03.142

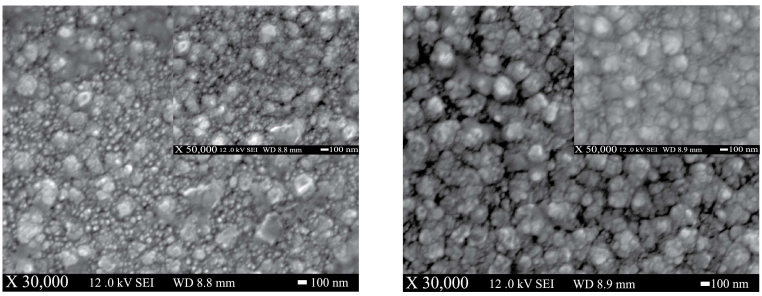

Fig. 8 (left) SEM images of the undoped ZnO thin film, (right) SEM images of the $Zn_{0.95}Mg0.05O$ thin films at 30k× and 50k×, big and small picture respectively.

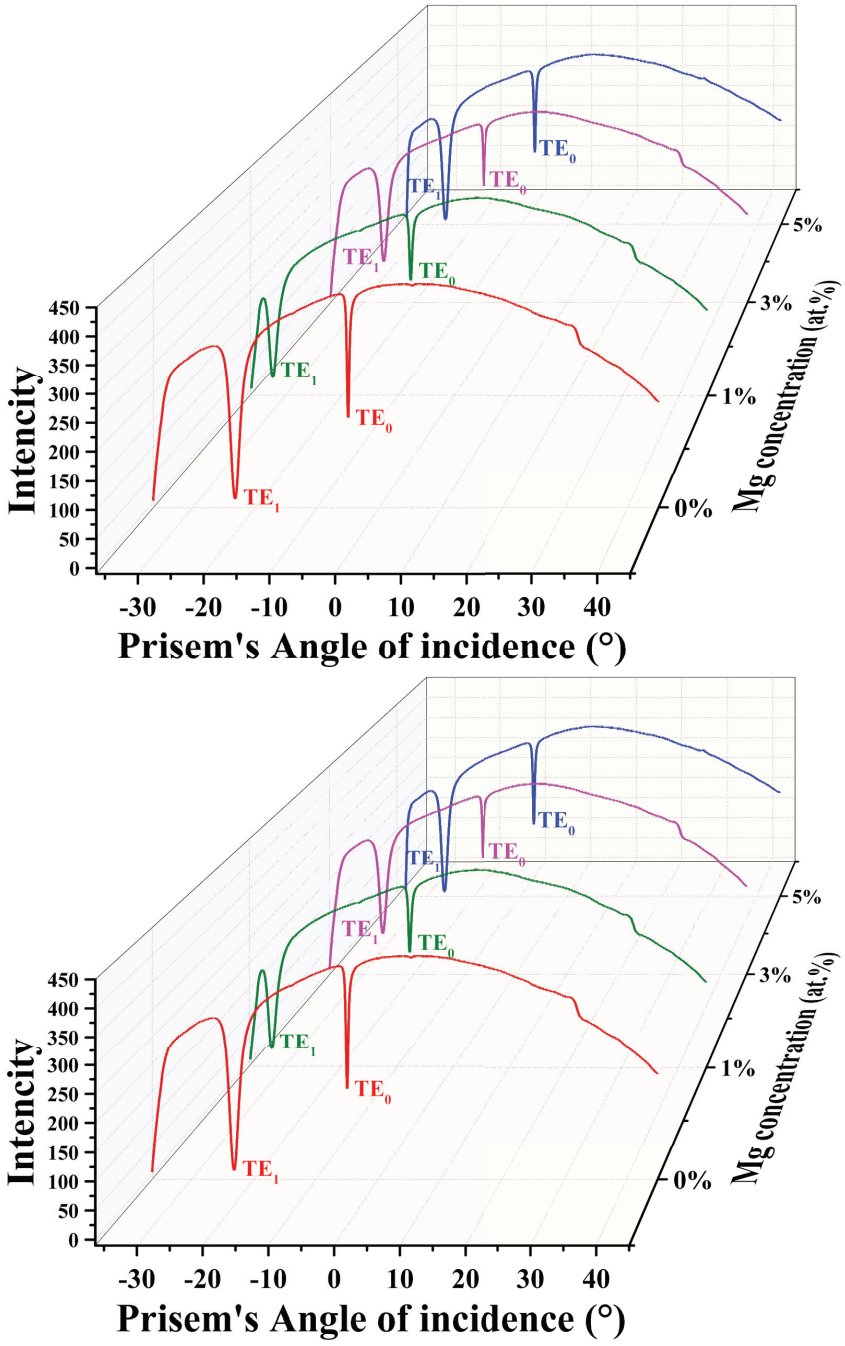

Fig. 9 M-lines intensity vs angle of incident for the deposited doped and undoped films in both Transverse Electric (TE) and Transverse Magnetic (TM).

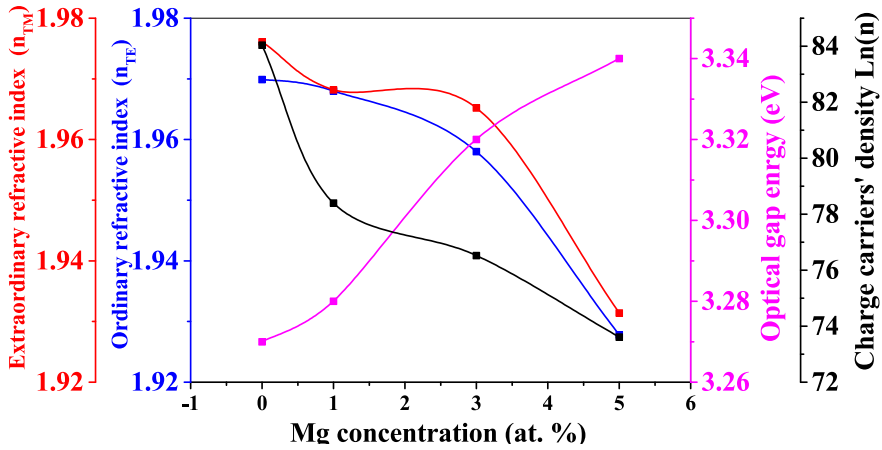

Fig. 10 Ordinary (n_{TE}) and extraordinary (n_{TM}) refractive indices, optical gap energy and charge carriers' density as a function of Mg concentration.

Figure

Click here to access/download;Figure;ZnO all MEB.eps

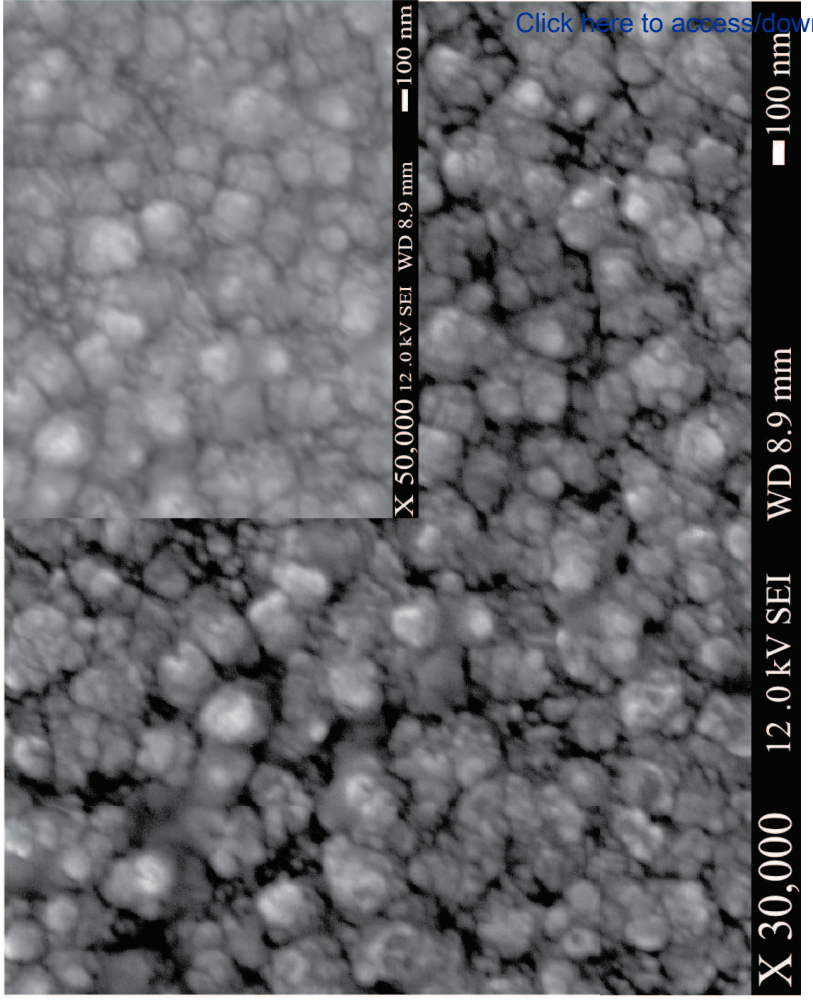

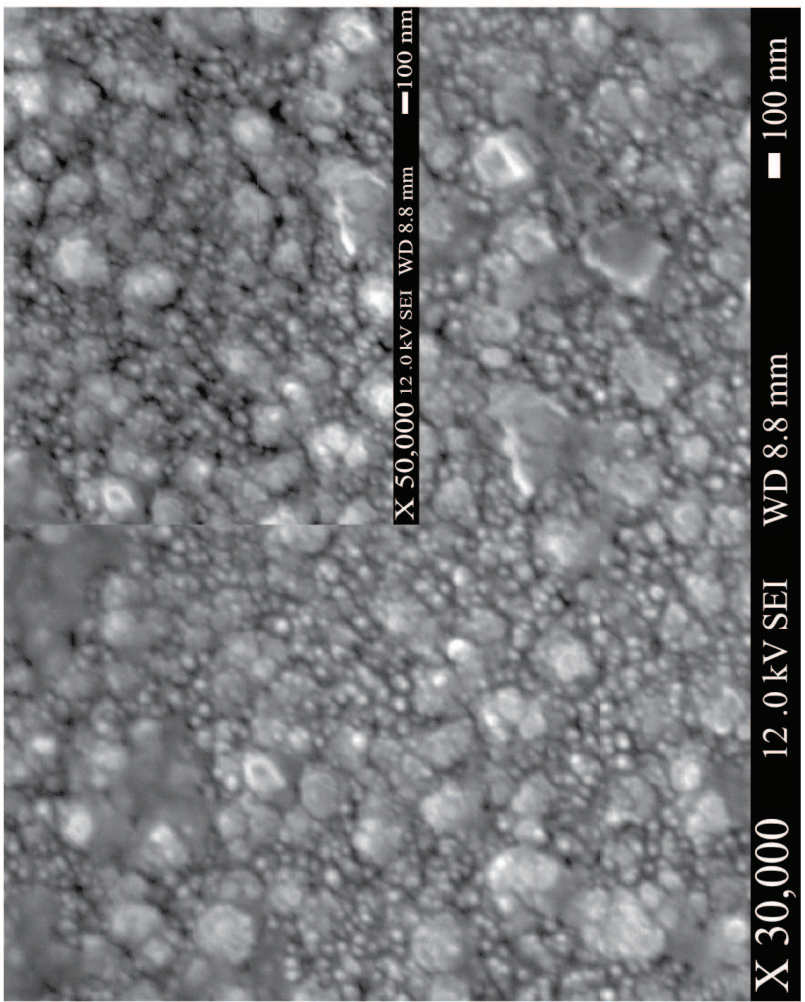

Optoelectronic and birefringence properties of weakly Mg doped ZnO thin films prepared by spray pyrolysis

Yassine Bouachiba[1], Abdelouadoud Mammeri[1*], Abderrahmane Bouabellou[1], Oualid Rabia[1], Saber Saidi[1], Adel Taabouche[1], Badis Rahal[1], Lyes Benharrat[1], Hacene Serrar[1] and Moukhtar Boudissa[1]

[1]Laboratoire Technologie des Matériaux Avancés,Ecole Nationale Polytechnique de Constantine Malek BENNABI,BP 75A RP,Ali Mendjeli, Constantine, Algérie.
[2*]Laboratoire Couches Minces et Interfaces, Université de Fréres Mentouri Constantine 1, Constantine, Algérie.
[3]Nuclear Techniques Division, Nuclear Research Center of Algiers, 2 Bd, Frantz Fanon, BP 399, 16000, Algiers, Algeria.
[4]Research Center in Semiconductors Technology for Energy-CRTSE, 02, Bd. Dr. Frantz Fanon, B.P. 140,7 Merveilles, 16038, Algiers, Algeria.
[5]Research Center in Industrial Technologies (CRTI), BP 64 Cheraga, Alger, Algeria.
[6]ENMC Laboratory, Department of Physics, Faculty of Science, University Ferhat Abbas, Setif, 19000, Algeria.

*Corresponding author(s). E-mail(s): abdelouadoud.mammeri@gmail.com;
Contributing authors: ybouachiba@gmail.com; a_bouabellou@yahoo.fr; oualidrabia28@gmail.com; saber18saidi@gmail.com; adelphm@gmail.com; b.rahal@crna.dz; benharrat.lyes@crtse.dz; serrarhacene@gmail.com; mokhtar.bousissa@univ-setif.dz;

1 Introduction

Zinc Oxide (ZnO) is is a multipurpose semiconductor with many uses such as ultra-capacitor electrode [**?**], spintronic devices [**?**], multigas sensing [**? ? ? ?**], piezoelectric devices [**?**], ultra-violet LEDs [**?**], detectors [**?**] as well as waveguides [**? ? ?**]. In its thin film form, ZnO has a large adaptation to several deposition methods such as chemical vapor deposition [**?**], pulsed laser deposition [**?**], spray pyrolysis [**?**], dip-coating [**?**] and electrochemical deposition [**?**]. ZnO has very interesting characteristics for application in electronics and optoelectronics devices, especially its exciton binding energy of 60 meV at 300K, a wide direct band gap of 3.37 eV [**?**]. In addition to an ordinary and extraordinary refractive indexes of $n_e = 2.006$ and $n_o = 1.990$ respectively [**?**]. To modify its electrical properties, ZnO was doped with Group III elements such as Al, Ga and In which acted as donor dopants to reinforce its n-type electrical nature and group V elements such as N, P, As and Sb which acted as acceptor dopants which changed ZnO to be a p-type semiconductor [**?**]. Controlling the refractive index of ZnO thin films was achieved by several ways including thermal annealing [**?**] and doping with In [**?**], Te, N [**?**] and Mg [**?**]. However, the effect of dopants on the optical and electrical properties of ZnO is still not well understood.

Tailoring ZnO optical and electrical properties via dopants while maintaining high quality films especially using spray pyrolysis is very attractive to both scientists and technology developers as it offers a control over several experimental parameters, it is cheap, uncomplicated and environmentally friendly.

Wurtzite $Mg_xZn_{1-x}O$ alloy is very interesting due to the high solubility of Mg in the ZnO wurtzite matrix (up to 30%) [**?**]. Moreover, it offers control over a range of optical and electrical properties of ZnO such as widening of the optical gap energy up to 0.85 eV [**?**], consequently, it can be used for multiple purposes such as a top layer in $Mg_xZn_{1-x}O$/ZnO multilayer UV photodetector [**?**] and high mobility MgZnO/ZnO thin film transistor [**?**] to name few. Concerning the waveguiding properties, little attention has been paid to wurtzite $Mg_xZn_{1-x}O$ as a waveguide, however, $Mg_xZn_{1-x}O$ was used as a buffer layer for ZnO waveguide thin film [**?**]. In an other work, a potential use of $Mg_xZn_{1-x}O$ cubic rocksalt-type phase as a wave guide was reported Yu et al. [**?**]. Wurtzite $Mg_xZn_{1-x}O$ thin film alloy refractive index was previously studied but there is still work to be done, as there are opposite results regarding the birefringence which is found to be negative in some studies [**? ?**] and positive in another study[**?**].

In this work, we engaged in the investigation of the relations between the refractive index, the optical gap energy and the charge carriers' density in addition to the birefringence of $Mg_xZn_{1-x}O$ thin films deposited by spray pyrolysis on glass substrate.

2 Results and Discussion

2.1 XRD analysis

From Figure **??**(a) we can see clearly that all films exhibit a crystalline hexagonal wurtzite structure (JCPDS card no. 00-036-1451) with the quasi-predominance of (002) peak indicating the preferential growth of undoped and Mg doped ZnO thin films through the c-axis direction. However, weak intensity peaks of other crystallographic directions were observed in the following positions 31.96°(100), 36.56°(101), 47.87°(102), 63.17°(103) and 72.85°(004). The peak (002) experienced a shift towards higher angles over Mg doping (Figure **??**(b)) which was reported by a number of authors [**? ? ?**] and it is due to the difference in the ionic radius between Mg^{+2} (0.57 Å) and Zn^{+2} (0.60 Å) [**?**]. This difference is directly related to the compression strain on the main axes of the wurtzite structure a and c. Previously, Chang et al. [**?**] reported also similar compression strain in their sputtered MgZnO thin films which were interpreted by good substitution between Mg and Zn ions.
The grain size can be calculated by Debye-Scherrer formula [**?**]:

$$D = \frac{K\lambda}{\beta \cos(\theta)} \tag{1}$$

where λ is the wavelength of the incident X-ray, θ is the Bragg's angle, K is the shape factor (0.9 for gaussian fit) and β is the Full Width at Half Maxima (FWHM) of the peaks. The crystallite size, lattice parameters and strain axes are tabulated in table **??**. It should be noted that there was no significant change in the average crystallite size (33.13 nm for Mg_0Zn_1O film and an average of 33.03 nm for the $Mg_xZn_{1-x}O$ films) and the minus sign of the strain values (ϵ_a and ϵ_c) approves the compression nature of the strain. To calculate lattice parameter c of the thin films we used the Bragg's law (with n=1) and the d spacing of wurtzite structure.

2.2 UV-Vis measurements

The transmittance of the thin films was slightly enhanced on average with the introduction of Mg in the visible region (400-800 nm). The limit of the absorption zone was shifted to smaller wavelengths which renders the thin films to be more dielectric as Mg doping is increased, this effect is directly related to the blue shift of the optical band gap and it was approximated for each film using the Tauc's plot:

$$\alpha h\nu = A(h\nu - E_g)^n \tag{2}$$

where $h\nu$ is the photon energy, E_g is the optical gap energy, A is constant and n equals $\frac{1}{2}$ since ZnO has a direct band gap. The widening of the optical band gap could be ascribed to the difference in electronegativity between Zn^{+2} and Mg^{+2} ions [**? ? ?**]. In similar study, Al-Ghamdi [**?**] reported this correlation

between the optical band gap energy and the electronegativity in his work about amorphous $Se_{96-x}Te_4Ag_x$ thin films.
In fact, it should be noted that both the electronegativity and electron affinity are directly related [**?**]. In this way Figure **??** presents the calculated optical band gap and the electron affinity versus Mg doping. The electron affinity ($e\chi$) was quantitatively calculated using Vegard's law [**?**]:

$$e\chi(Mg_xZn_{1-x}O) = e\chi(ZnO) - (e\chi(ZnO) - e\chi(MgO))x \quad (3)$$

$e\chi(ZnO)$, $e\chi(MgO)$ have the value of 4.5 eV [**?**] and 0.85 eV [**?**] for the electron affinity of ZnO and MgO respectively. Previously, iskenderoglu et al. [**?**] approved experimentally by UPS technique the inverse relation between the optical gap energy and the electron affinity of sprayed MgZnO alloy thin film, with Mg doping ranging from 0 to 15%.

2.3 Photoluminescence

The room temperature photoluminescence spectra are shown in Figure **??**. The undoped thin film had four peaks at 381 (3.25 eV), 416 (2.98 eV), 441 (2.81 eV) and 505 nm (2.46 eV) which were explained by: the emission corresponding to excitons recombination, zinc interstitial (Zn_i), oxygen vacancies (V_O) and donor V_O – acceptor V_{Zn} recombination respectively [**? ?**]. The same peaks were observed also in $Mg_{0.01}Zn_{0.99}O$ except a blue shift of the 380 peak to 381 nm (3.26 eV). The $Mg_{0.03}Zn_{0.97}O$ thin film had three peaks 379 (3.27 eV), 416 (2.81 eV) and 492 nm (2.52 eV) and they were attributed to excitons recombination, zinc interstitial (Zn_i) [**?**] and oxygen vacancy (V_O) [**?**] respectively. Finally the $Mg_{0.05}Zn_{0.95}O$ thin film exhibited two peaks at 378 (3.28 eV) and 503 nm (2.47 eV) and they were manifestations of excitons and donor V_O – acceptor V_{Zn} recombinations [**? ?**]. The blue shift of the near band edge emission from the PL peaks was in consistency with the UV visible calculations of the optical band gap, however, it was at a lower rate which was explained by stokes shift [**?**].

2.4 Electrical measurements

Figure **??** demonstrates the near isotropic electric transportation of the deposited films which could be attributed to the fact that the films have the predominant orientation (002) of the wurtzite structure [**?**].
The free charge carriers' density decreased from 3.146×10^{18} for the undoped film to 9.273×10^{13} cm^{-3} for $Mg_{0.05}Zn_{0.95}O$ film. In parallel, the resistivity increased from 109 to 1268 Ω cm and the mobility increased from 0.01821 to 53.08 $cm^2/(V.s)$. The decreased charge carriers' density could be attributed to the fact that the conduction band (CB) of pure ZnO consists mainly of O_{2p} and Zn_{4s} states [**? ?**], so the introduction of Mg in ZnO thin films will reduce the Zn_{4s} state and introduce Mg_{3p} state which has high energy relative to the Zn_{4s} [**? ?**]. Moreover, the widening in the optical bang gap energy discussed

previously, could also influence the free charge carriers' density since the electrons passing from the valance band must requires higher energy to access the conduction band.

2.5 Surface morphology

Figure **??** shows the morphology of undoped and 5 at. % doped ZnO thin films. The undoped (Figure **??**(a)) thin film shows a dense surface with granular mixture of small grains and large aggregates. The size of the small grains varies from $\sim$ 20 to 80 nm and that of the aggregates reaches $\sim$ 200-300 nm. From the doped sample (Figure **??**(b)), it is evident that magnesium has a tendency to promote the phenomenon of coalescence. This doped film shows a less dense and relatively homogeneous morphology with large aggregates whose size varies from $\sim$ 200 to 500 nm.
No cracks nor empty holes were observed on the surface of the films, revealing the high quality of our films.

2.6 M-lines measurements

The M-lines measurements demonstrated the guiding modes present in the films. All films had four guiding modes (TE_0, TE_1, TM_0, and TM_1) two for each optical polarization (Transverse Electric mode (TE) and Transverse Magnetic mode (TM)) as illustrated in Figure **??**. Using the dispersion equations for TE and TM polarizations, the optogeometric parameters can be calculated [**?** **?** **?**]. The effective indices, the films thicknesses and the birefringence values are presented in Table **??**.
Figure **??** illustrate the variation of n_{TE}, n_{TM}, optical gap energy and free charge carriers' density as a function of the Mg concentration. The slight difference between n_{TM} and n_{TE} confirmed the birefringence behavior of our films. This made the guided waves traveling during the TE mode in the plane perpendicular to the *c*-axis of the wurtzite structure submit to an ordinary refractive index (n_{TE}) and during the TM mode to an extraordinary one (n_{TM}) [**?**]. Both n_{TE} and n_{TM} were found to decreased over Mg doping. This behavior seems to be in good agreement with the broadening of the optical band gap and the depletion of the conduction band free charge carriers' (Figure **??**) [**?**]. The birefringence was measured to be positive for all films which is a good indication for the unchanging orientations of the bonds Zn-O with the replacement of Zn by Mg [**?** **?**].
The inverse relation between the optical gap energy, the resistivity and the refractive index as Mg content increased in the ZnO thin film was also observed by Kaushal et al. [**?**]. The same fact has been reported by Teng et al. [**?**] for Mg-doped ZnO thin films prepared by pulsed laser deposition. In similar study, Sorar et al. [**?**] found that the ordinary refractive index generally decreases with the increase of the Si doping in ZnO thin films prepared by sol-gel and annealed at 350 °C and 550 °C whereas their optical band gap energy was found to be blue shifted.

3 Tables

4 Figures

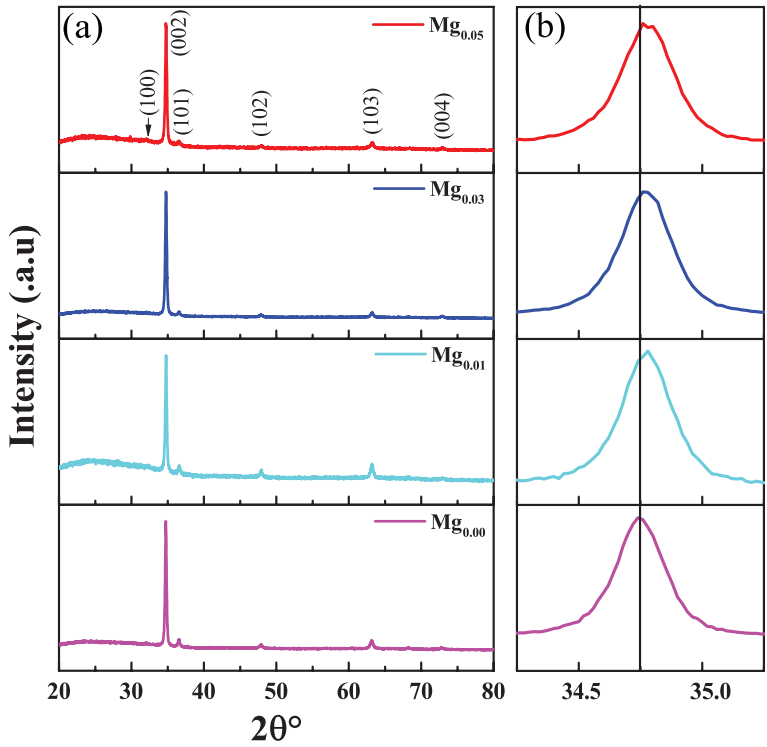

Fig. 1 (a) XRD spectra of undoped and Mg doped ZnO thin films, (b) an emphasis of the (002) peak showing a shift towards higher angles for the doped thin films.

5 Methods

The sprayed solution for the undoped ZnO thin films was prepared by dissolving the proper amount of dihydrate zinc acetate [$Zn(CH_3CO_2)_2 \cdot 2H_2O$] in 99.98% pure methanol to obtain 0.1 M solution that was submitted to a constant stirring at 60 °C for 45 min on a magnetic stirrer. Concerning the sprayed solution of the Mg doped ZnO thin films, we maintained the same parameters with the use of magnesium chloride [$Mg(CH_3CO_2)_2 \cdot 4H_2O$] as Mg precursor and each time the proper amount was added to 0.1 M methanol solutions of $Zn(CH_3CO_2)_2 \cdot 2H_2O$ to produce the following contents of zinc and magnesium: $Mg_xZn_{1-x}O$ with x equals 0.01, 0.03 and 0.05.

An ordinary glass substrate were ultra-sonically cleaned in a 1:1 mixture of acetone and ethanol for 15 min and left to dry in air. The films were deposited

Table 1 The information obtained and calculated from the XRD spectra.

Sample	2θ (degree)	d spacing (Å)	Crystallite size (nm)	a(Å)	c(Å)	ϵ_a (10^{-3})	ϵ_c (10^{-3})
$Mg_{0.00}Zn_{1.00}O$	34.75	2.580	33.13	3.2306	5.1592	-3.4241	-5.4746
$Mg_{0.01}Zn_{0.99}O$	34.77	2.455	31.26	3.2240	5.1560	-5.4601	-6.0915
$Mg_{0.03}Zn_{0.97}O$	34.77	2.456	31.30	3.2256	5.1560	-4.9665	-6.0915
$Mg_{0.05}Zn_{0.95}O$	34.78	2.577	35.83	3.2298	5.1547	-3.6709	-6.3421

Table 2 Optogeometric Properties of the deposited thin films.

Sample	Effective index $\pm 10^{-4}$				Refractive index 10^{-4}		Thickness TE	Thickness TM	Birefringence
	TE_0	TE_1	TM_0	TM_1	n_{TE}	n_{TM}	$\pm 0.1nm$	$\pm 0.1nm$	$(n_{TM} - n_{TE})$
$Mg_{0.00}Zn_1.00O$	1.8923	1.6565	1.8793	1.6033	1.9699	1.9761	436.1	452.1	0.0062
$Mg_{0.01}Zn_{0.99}O$	1.8758	1.5994	1.8539	1.5486	1.9680	1.9682	347.4	382.6	0.0002
$Mg_{0.03}Zn_{0.97}O$	1.8738	1.6203	1.8581	1.5647	1.9580	1.9652	413.1	426.3	0.0072
$Mg_{0.05}Zn_{0.95}O$	1.8451	1.5981	1.8278	1.5494	1.9278	1.9314	417.7	433.7	0.0036

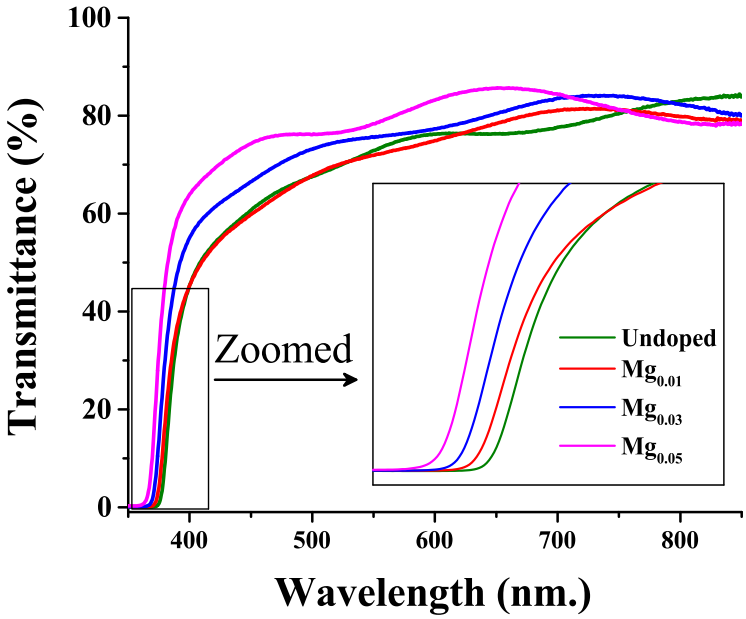

Fig. 2 Transmittance spectra of pure and doped ZnO thin films zoomed in the absorption region.

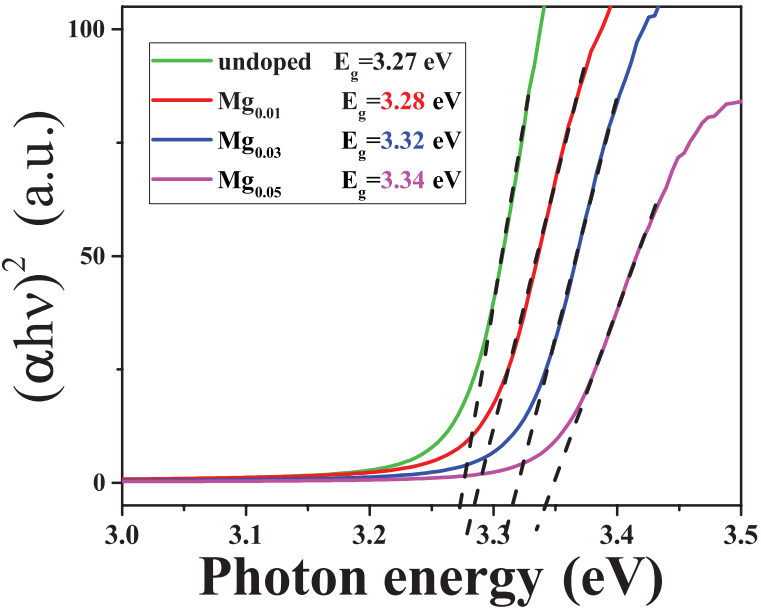

Fig. 3 Tauc's plot for the undoped and doped ZnO thin films.

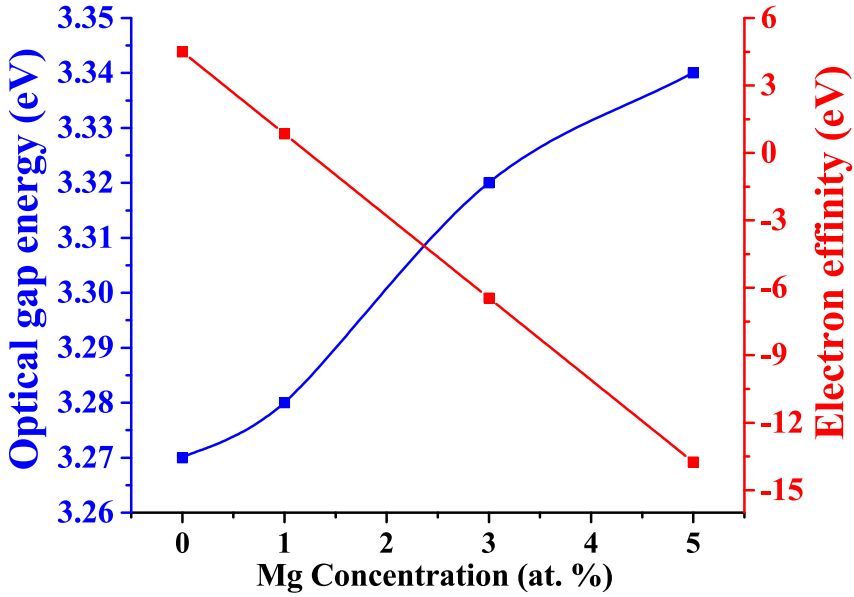

Fig. 4 The evolution of the optical band gap energy and the electron affinity of $Mg_xZn_{1-x}O$ thin films as a function of Mg concentration.

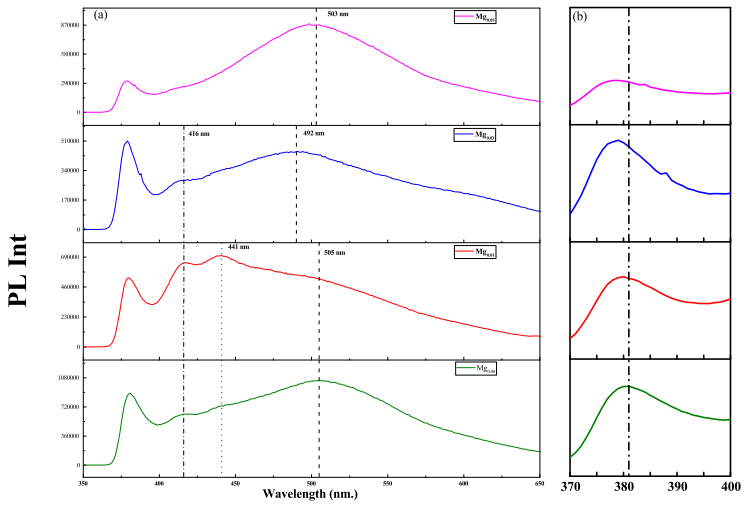

Fig. 5 (a) Room temperature photoluminescence spectra, (b) an emphasis of the excitons recombination peaks.

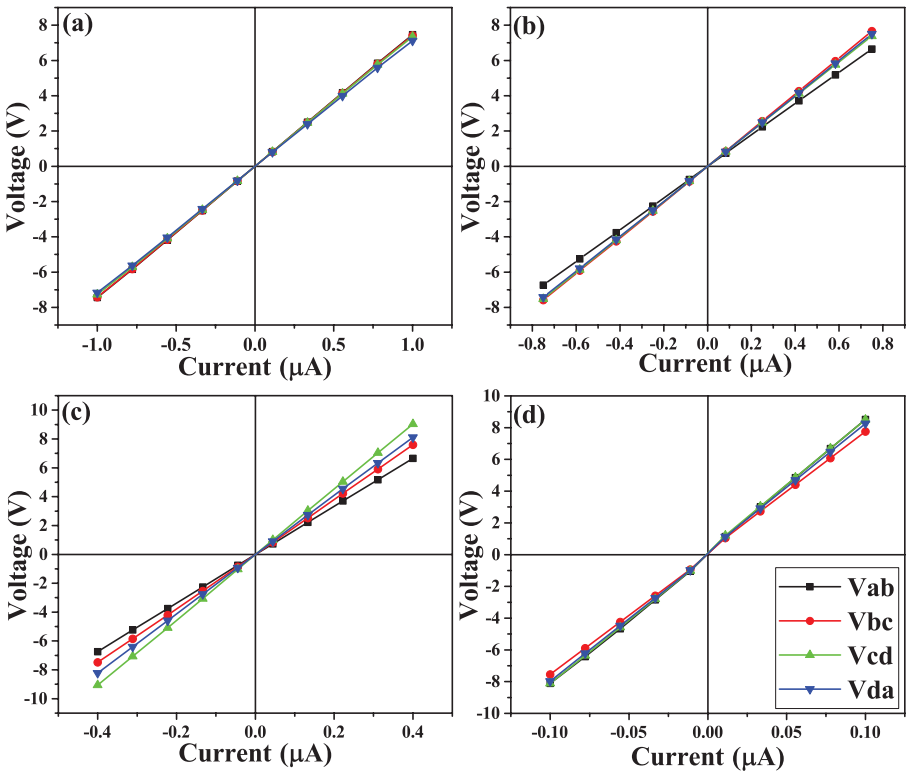

Fig. 6 I-V measurements for the four thin films: (a) undoped ZnO, (b) $Mg_{0.01}Zn_{0.99}O$, (c) $Mg_{0.03}Zn_{0.97}O$ and (d) $Mg_{0.05}Zn_{0.95}O$.

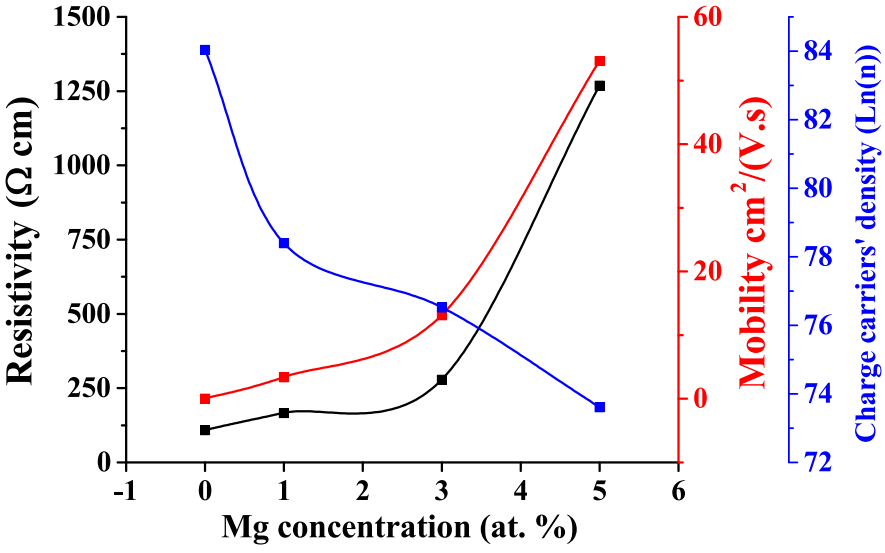

Fig. 7 Resistivity (ρ) and charge carriers (n) as a function of Mg concentration.

using spray pyrolysis system. The deposition temperature was 450 °C.
In order to characterize our thin films, multiple techniques were used: Philips PANalytical X'Pert Pro diffractometer with a wave length of 1.5406 Å, environmental scanning electron microscope Philips XL30 ESEM FEG and for the electrical properties Ecopia HMS-3000 hall effect measurement system, finally for the optical measurements, Metricon 2010/M Prism (rutile TiO_2: n_e=2,8639 and n_o=2.5822 at 632,8 nm with an apical angle of 44,60 °) Coupler was used to couple 632.8 nm HeNe laser light into air/$Mg_xZn_{1-x}O$/glass waveguide and Shimadzu UV-3101PC Spectrophotometer.

6 Conclusion

Mg doped ZnO thin films were successfully deposited on glass substrate via spray pyrolysis at 450 °C. The XRD characterization showed highly *c* oriented thin films with a decrease in *a* and *c* as the Mg concentration increased in the thin films. The undoped thin film had a multisize grain distribution meanwhile the $Mg_{0.05}Zn_{0.95}O$ had a more homogeneous grain distribution. Mg doping in the ZnO films led to a blue shift of the optical band gap energy and a depletion of the conduction band due to the drop in free carriers' density that had a direct effect on the ordinary and the extraordinary refractive indexes that were found to decrease. The birefringence of a crystal depends on multiple factors such as strain, defects charge carriers' density, bounds orientations and so on, therefore it will change from papers to papers with the change of deposition method especially.

Declarations

- Funding: Not applicable
- Conflict of interest/Competing interests: The authors declare that they have no conflict of interest.
- Ethics approval: Not applicable
- Consent to participate: Not applicable
- Consent for publication: Not applicable
- Availability of data and materials: Not applicable
- Code availability: Not applicable
- Authors' contributions: Not applicable

References

[1] Lakshmi, K., Revathi, S.: Rice-like zno architecture: An eminent electrode material for high-performance ultracapacitor application. Journal of Inorganic and Organometallic Polymers and Materials **31**(5), 1992–2002 (2021). https://doi.org/10.1007/s10904-021-01922-5

[2] Pearton, S., Norton, D., Heo, Y., Tien, L.-C., Ivill, M., Li, Y., Kang, B., Ren, F., Kelly, J., Hebard, A.: Zno spintronics and nanowire devices.

Journal of Electronic Materials **35**, 862–868 (2006). https://doi.org/10.1007/BF02692541

[3] Hosseinnejad, M.T., Shirazi, M., Ghoranneviss, M., Hantehzadeh, M.R., Darabi, E.: Preparation of nanostructured zno thin films using magnetron sputtering for the gas sensors applications. Journal of Inorganic and Organometallic Polymers and Materials **26**(2), 405–412 (2016). https://doi.org/10.1007/s10904-015-0324-0

[4] Hjiri, M., Bahanan, F., Aida, M., El Mir, L., Neri, G.: High performance co gas sensor based on zno nanoparticles. Journal of Inorganic and Organometallic Polymers and Materials **30**(10), 4063–4071 (2020). https://doi.org/10.1007/s10904-020-01553-2

[5] Blauw, M., Dam, V.A., Crego-Calama, M., Brongersma, S., Musschoot, J., Detavernier, C.: Oxygen sensing with zno thin films. Proceedings of IEEE Sensors **28–31**, 1416–1419 (2011). https://doi.org/10.1109/ICSENS.2011.6127128

[6] Patil, V.L., Vanalakar, S.A., Patil, P.S., Kim, J.H.: Fabrication of nanostructured zno thin films based no2 gas sensor via silar technique. Sensors and Actuators B: Chemical **239**, 1185–1193 (2017). https://doi.org/10.1016/j.snb.2016.08.130

[7] Polewczyk, V., Maffei, R., Vinai, G., Cicero, M., Prato, S., Capaldo, P., Zilio, S., Bona, A., Paolicelli, G., Mescola, A., D'Addato, S., Torelli, P., Benedetti, S.: Zno thin films growth optimization for piezoelectric application. Sensors **21**, 6114 (2021). https://doi.org/10.3390/s21186114

[8] Sandeep, K.M., Bhat, S., Dharmaprakash, S.M.: Structural, optical, and led characteristics of zno and al doped zno thin films. Journal of Physics and Chemistry of Solids **104**, 36–44 (2017). https://doi.org/10.1016/j.jpcs.2017.01.003

[9] Shaikh, S., Ganbavle, V., Inamdar, S., Rajpure, K.: Multifunctional zinc oxide thin films for high performance uv photodetector and nitrogen dioxide gas sensor. RSC Adv. **6** (2016). https://doi.org/10.1039/C6RA01750A

[10] Kamauchi, M., Shiosaki, T., Kawabata, A.: Channel optical waveguides of zno thin films. In: [Proceedings] 1990 IEEE 7th International Symposium on Applications of Ferroelectrics, pp. 733–736 (1990). https://doi.org/10.1109/ISAF.1990.200361

[11] Yu, S.F., Yuen, C., Lau, S.P., Fan, W.J.: Design and fabrication of zinc oxide thin-film ridge waveguides on silicon substrate with ultraviolet amplified spontaneous emission. IEEE Journal of Quantum Electronics

40(4), 406–412 (2004). https://doi.org/10.1109/JQE.2004.825212

[12] Teraoka, E., Kita, T., Tsukazaki, A., Kawasaki, M., Yamada, H.: Fabrication of zno channel waveguides for nonlinear optical applications. Proceedings of SPIE - The International Society for Optical Engineering **7940** (2011). https://doi.org/10.1117/12.874439

[13] Chen, Z., Shum, K., Salagaj, T., Zhang, W., Strobl, K.: Zno thin films synthesized by chemical vapor deposition, pp. 1–6 (2010). https://doi.org/10.1109/LISAT.2010.5478331

[14] Shan, F.K., Shin, B.C., Jang, S.W., Yu, Y.S.: Substrate effects of zno thin films prepared by pld technique. Journal of the European Ceramic Society **24**(6), 1015–1018 (2004). https://doi.org/10.1016/S0955-2219(03)00397-2. Electroceramics VIII

[15] Lehraki, N., Aida, M.S., Abed, S., Attaf, N., Attaf, A., Poulain, M.: Zno thin films deposition by spray pyrolysis: Influence of precursor solution properties. Current Applied Physics **12**(5), 1283–1287 (2012). https://doi.org/10.1016/j.cap.2012.03.012

[16] Rahal, B., Boudine, B., Larbah, Y., Siad, M., Souami, N.: Influence of low cd-doping concentration (0.5 and 3 wt.%) and different substrate types (glass and silicon) on the properties of dip-coated nanostructured zno semiconductors thin films. Journal of Inorganic and Organometallic Polymers and Materials, 1–17 (2021). https://doi.org/10.1007/s10904-021-02024-y

[17] Hamidi, A.S., Abidin, M.S.Z.: Electrochemical deposition of zinc oxide thin film using two-terminal setup. In: 2017 IEEE Regional Symposium on Micro and Nanoelectronics (RSM), pp. 34–37 (2017). https://doi.org/10.1109/RSM.2017.8069136

[18] Ellmer, K., Klein, A., Rech, B. (eds.): Transparent Conductive Zinc Oxide: Basics and Applications in Thin Film Solar Cells. Springer series in materials science, vol. 104. Springer, Berlin (2008). OCLC: ocn181423059

[19] Mehan, N., Tomar, M., Gupta, V., Mansingh, A.: Optical waveguiding and birefringence properties of sputtered zinc oxide (zno) thin films on glass. Optical Materials **27**(2), 241–248 (2004). https://doi.org/10.1016/j.optmat.2004.03.005

[20] Jagadish, C., Pearton, S.J.: Zinc Oxide Bulk, Thin Films and Nanostructures: Processing, Properties, and Applications vol. 7. Elsevier, ??? (2011)

[21] Huang, B., Li, J., Wu, Y.-b., Guo, D.-h., Wu, S.-t.: Optical constants of

transparent zno films by rf magnetron sputtering. Materials Letters **62**(8), 1316–1318 (2008). https://doi.org/10.1016/j.matlet.2007.08.043

[22] Xie, G.C., Fanga, L., Peng, L.P., Liu, G.B., Ruan, H.B., Wu, F., Kong, C.Y.: Effect of In-doping on the Optical Constants of ZnO Thin Films. Physics Procedia **32**, 651–657 (2012). https://doi.org/10.1016/j.phpro.2012.03.614. Accessed 2021-07-23

[23] Cai, A.L., Muth, J.F., Porter, H.L., Kvit, A., Narayan, J.: The refractive index and other properties of doped zno films. MRS Proceedings **764**, 3–21 (2003). https://doi.org/10.1557/PROC-764-C3.21

[24] Teng, C., Muth, J., Ozgur, U., Bergmann, M., Everitt, H., Sharma, A., Jin, C., Narayan, J.: Refractive indices and absorption coefficients of mgxzn1-xo alloys. Applied Physics Letters **76**, 979–981 (2000). https://doi.org/10.1063/1.125912

[25] iskenderoglu, D., Kasapoglu, A., Gür, E.: Valance band properties of mgzno thin films with increasing mg content; phase separation effects. Materials Research Express **6** (2018). https://doi.org/10.1088/2053-1591/aaf45e

[26] Özgür, ., Alivov, Y.I., Liu, C., Teke, A., Reshchikov, M.A., Doğan, S., Avrutin, V., Cho, S.-J., Morkoç, H.: A comprehensive review of zno materials and devices. Journal of Applied Physics **98**(4), 041301 (2005) https://arxiv.org/abs/https://doi.org/10.1063/1.1992666. https://doi.org/10.1063/1.1992666

[27] Rana, V.S., Rajput, J.K., Pathak, T.K., Purohit, L.P.: Multilayer mgzno/zno thin films for uv photodetectors. Journal of Alloys and Compounds **764**, 724–729 (2018). https://doi.org/10.1016/j.jallcom.2018.06.139

[28] Yue, D., Guo, S., Han, S., Cao, P., Zeng, Y., Xu, W., Fang, M., Liu, W., Zhu, D., Lu, Y., Qian, Y.: Facile fabrication of mgzno/zno composites for high performance thin film transistor. Journal of Alloys and Compounds **873**, 159840 (2021). https://doi.org/10.1016/j.jallcom.2021.159840

[29] Jia, C.-L., Wang, K.-M., Wang, X.-L., Zhang, X.-J., Lu, F.: Formation of c-axis oriented zno optical waveguides by radio-frequency magnetron sputtering. Optics express **13**, 5093–9 (2005). https://doi.org/10.1364/OPEX.13.005093

[30] Yu, P., Wu, H.Z., Xu, T.N., Qiu, D.J., Hu, G.J., Dai, N.: Cubic phase mgxzn1-xo thin films for optical waveguides. Journal of Crystal Growth **310**(2), 336–340 (2008). https://doi.org/10.1016/j.jcrysgro.2007.10.028

[31] Morkoç, H., Özgür, m.: Zinc Oxide: Fundamentals, Materials and Device Technology, 1st edn. Wiley, ??? (2009). https://doi.org/10.1002/9783527623945. https://onlinelibrary.wiley.com/doi/book/10.1002/9783527623945 Accessed 2021-07-26

[32] Khorramshahi, V., Karamdel, J., Yousefi, R.: Acetic acid sensing of Mg-doped ZnO thin films fabricated by the sol–gel method. Journal of Materials Science: Materials in Electronics **29**(17), 14679–14688 (2018). https://doi.org/10.1007/s10854-018-9604-0. Accessed 2021-06-18

[33] Kim, T.H., Park, J.J., Nam, S.H., Park, H.S., Cheong, N.R., Song, J.K., Park, S.M.: Fabrication of Mg-doped ZnO thin films by laser ablation of Zn:Mg target. Applied Surface Science **255**(10), 5264–5266 (2009). https://doi.org/10.1016/j.apsusc.2008.07.105. Accessed 2021-06-18

[34] Shan, F.K., Kim, B.I., Liu, G.X., Liu, Z.F., Sohn, J.Y., Lee, W.J., Shin, B.C., Yu, Y.S.: Blueshift of near band edge emission in Mg doped ZnO thin films and aging. Journal of Applied Physics **95**(9), 4772–4776 (2004). https://doi.org/10.1063/1.1690091. Accessed 2021-06-18

[35] Rouchdi, M., Salmani, E., Fares, B., Hassanain, N., Mzerd, A.: Synthesis and characteristics of Mg doped ZnO thin films: Experimental and ab-initio study. Results in Physics **7**, 620–627 (2017). https://doi.org/10.1016/j.rinp.2017.01.023. Accessed 2021-06-18

[36] Chang, R.-C., Chu, S.-Y., Yeh, P.-W., Hong, C.-S., Kao, P.-C., Huang, Y.-J.: The influence of Mg doped ZnO thin films on the properties of Love wave sensors. Sensors and Actuators B: Chemical **132**(1), 290–295 (2008). https://doi.org/10.1016/j.snb.2008.01.038. Accessed 2021-06-18

[37] Hussain, F., Imran, M., Khalil, R.M.A., Niaz, N.A., Rana, A.M., Sattar, M.A., Ismail, M., Majid, A., Kim, S., Iqbal, F., Javid, M.A., Saeed, S., Sattar, A.: An insight of Mg doped ZnO thin films: A comparative experimental and first-principle investigations. Physica E: Low-dimensional Systems and Nanostructures **115**, 113658 (2020). https://doi.org/10.1016/j.physe.2019.113658. Accessed 2021-06-18

[38] Huang, K., Tang, Z., Zhang, L., Yu, J., Lv, J., Liu, X., Liu, F.: Preparation and characterization of Mg-doped ZnO thin films by sol–gel method. Applied Surface Science **258**(8), 3710–3713 (2012). https://doi.org/10.1016/j.apsusc.2011.12.011. Accessed 2021-06-18

[39] Agrawal, A., Dar, T.A., Sen, P., Phase, D.M.: Transport and magneto-transport study of Mg doped ZnO thin films. Journal of Applied Physics **115**(14), 143701 (2014). https://doi.org/10.1063/1.4870864. Accessed 2021-06-18

[40] Al-Ghamdi, A.A.: Optical band gap and optical constants in amorphous Se96-xTe4Agx thin films. Vacuum **80**(5), 400–405 (2006). https://doi.org/10.1016/j.vacuum.2005.07.003. Accessed 2021-09-18

[41] Mulliken, R.S.: A New Electroaffinity Scale; Together with Data on Valence States and on Valence Ionization Potentials and Electron Affinities. The Journal of Chemical Physics **2**(11), 782–793 (1934). https://doi.org/10.1063/1.1749394. Accessed 2021-09-17

[42] Vegard, L.: Die konstitution der mischkristalle und die raumfüllung der atome. Zeitschrift für Physik **5**(1), 17–26 (1921)

[43] Hussain, B., Aslam, A., Khan, T.M., Creighton, M., Zohuri, B.: Electron affinity and bandgap optimization of zinc oxide for improved performance of zno/si heterojunction solar cell using pc1d simulations. Electronics **8**(2), 238 (2019)

[44] Aboelfotoh, M.O., Lorenzen, J.A.: Influence of secondary-electron emission from mgo surfaces on voltage-breakdown curves in penning mixtures for insulated-electrode discharges. Journal of Applied Physics **48**(11), 4754–4759 (1977) https://arxiv.org/abs/https://doi.org/10.1063/1.323490. https://doi.org/10.1063/1.323490

[45] Mishra, S., Srivastava, R., Prakash, S., Yadav, R., Panday, A.: Photoluminescence and photoconductive characteristics of hydrothermally synthesized zno nanoparticles. Opto-Electronics Review **18**(4), 467–473 (2010)

[46] Chen, H., Ding, J., Guo, W., Chen, G., Ma, S.: Blue-green emission mechanism and spectral shift of al-doped zno films related to defect levels. RSC Adv. **3**, 12327–12333 (2013). https://doi.org/10.1039/C3RA40750K

[47] Babu, K.S., Reddy, A.R., Sujatha, C., Reddy, K.V., Mallika, A.: Synthesis and optical characterization of porous zno. Journal of Advanced Ceramics **2**(3), 260–265 (2013)

[48] Kim, T.H., Park, J.J., Nam, S.H., Park, H.S., Cheong, N.R., Song, J.K., Park, S.M.: Fabrication of mg-doped zno thin films by laser ablation of zn: Mg target. Applied Surface Science **255**(10), 5264–5266 (2009)

[49] Oliveira, M., Castro, A., Marques, M., Rubio, A.: On the use of neumann's principle for the calculation of the polarizability tensor of nanostructures. Journal of nanoscience and nanotechnology **8**, 3392–8 (2008). https://doi.org/10.1166/jnn.2008.142

[50] Hu, Y., Zeng, H., Du, J., Hu, Z., Zhang, S.: The structural, electrical and optical properties of mg-doped ZnO with different interstitial mg

concentration. Materials Chemistry and Physics **182**, 15–21 (2016). https://doi.org/10.1016/j.matchemphys.2016.05.065. Accessed 2021-06-29

[51] Bustanafruz, F., Fazli, M., Mohammadizadeh, M.R., Jafar Tafreshi, M.: Optical and electronic properties of h-doped ZnO. Optical and Quantum Electronics **48**(5), 297 (2016). https://doi.org/10.1007/s11082-016-0575-1. Accessed 2021-06-29

[52] Wang, J., Tu, Y., Yang, L., Tolner, H.: Theoretical investigation of the electronic structure and optical properties of zinc-doped magnesium oxide. Journal of Computational Electronics **15**, 1521–1530 (2016). https://doi.org/10.1007/s10825-016-0906-2

[53] Zheng, W., Feng, Z.C., Chang, F.H., Lee, J.F., Zheng, R.S., Wuu, D.S., Liu, C.W.: Study of $Mg_xZn_{1-x}O$ Alloys ($0<x<0.15$) by X-Ray Absorption Spectroscopy. Advanced Materials Research **663**, 361–365 (2013). https://doi.org/10.4028/www.scientific.net/AMR.663.361. Accessed 2021-07-29

[54] Bouachiba, Y., Taabouche, A., Bouabellou, A., Hanini, F., Sedrati, C., Merabti, H.: Tio waveguides thin films prepared by sol-gel method on glass substrates with and without zno underlayer. Materials Science-Poland **38**(3), 381–385 (2020). https://doi.org/10.2478/msp-2020-0043

[55] Medjaldi, F., Bouabellou, A., Bouachiba, Y., Taabouche, A., Bouatia, K., Serrar, H.: Study of TiO2, SnO2 and nanocomposites TiO2:SnO2 thin films prepared by sol-gel method: Successful elaboration of variable–refractive index systems **7**(1), 016439 (2020). https://doi.org/10.1088/2053-1591/ab6c0c

[56] Gharbi, B., Taabouche, A., Brella, M., Gheriani, R., Bouachiba, Y., Bouabellou, A., Hanini, F., Barouk, S.L., Serrar, H., Rahal, B.: Spray pyrolysis synthesized and zno–nio nanostructured thin films analysis with their nanocomposites for waveguiding applications. Semiconductors **55**, 37–43 (2021)

[57] Feynman, R.P., Leighton, R.B., Sands, M.: The Feynman Lectures on Physics; New Millennium Ed. Basic Books, New York, NY (2010). Originally published 1963-1965. https://cds.cern.ch/record/1494701

[58] Weber, H.-J.: Anisotropic bond polarizabilities in birefringent crystals. Acta Crystallographica Section A **44**(3), 320–326 (1988). https://doi.org/10.1107/S0108767387012492

[59] Lidin, S.: Mapping bond orientations with polarized x-rays. Science **344**(6187), 969–970 (2014). https://doi.org/10.1126/science.1254902

[60] Kaushal, A., Kaur, D.: Effect of mg content on structural, electrical and

optical properties of zn1-xmgxo nanocomposite thin films. Solar Energy Materials and Solar Cells **93**, 193–198 (2009). https://doi.org/10.1016/j.solmat.2008.09.039

[61] Sorar, I., Saygin-Hinczewski, D., Hinczewski, M., Tepehan, F.Z.: Optical and structural properties of si-doped zno thin films. Applied Surface Science **257**(16), 7343–7349 (2011). https://doi.org/10.1016/j.apsusc.2011.03.142

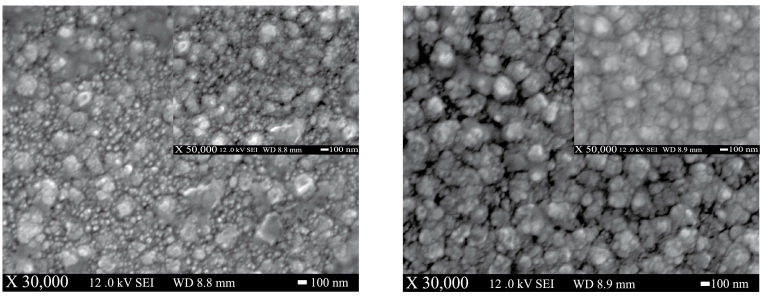

Fig. 8 (left) SEM images of the undoped ZnO thin film, (right) SEM images of the $Zn_{0.95}Mg0.05O$ thin films at 30k× and 50k×, big and small picture respectively.

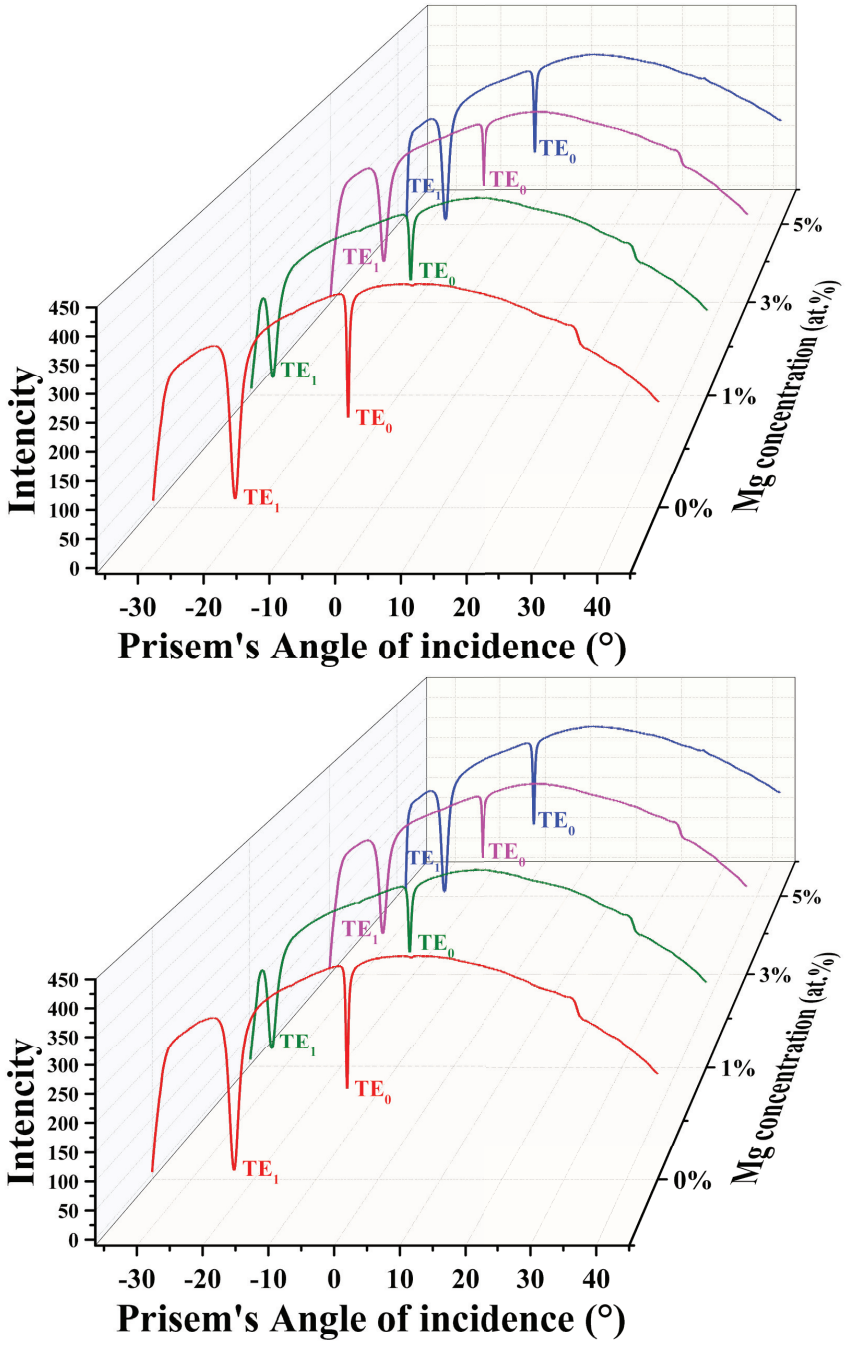

Fig. 9 M-lines intensity vs angle of incident for the deposited doped and undoped films in both Transverse Electric (TE) and Transverse Magnetic (TM).

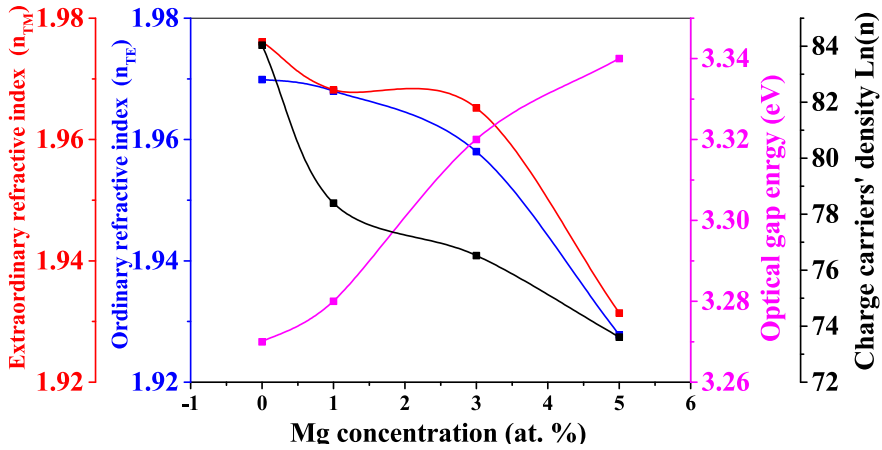

Fig. 10 Ordinary (n_{TE}) and extraordinary (n_{TM}) refractive indices, optical gap energy and charge carriers' density as a function of Mg concentration.

Optoelectronic and birefringence properties of weakly Mg doped ZnO thin films prepared by spray pyrolysis

Yassine Bouachibaa[1], Abdelouadoud Mammeri[2*], Abderrahmane Bouabellou[2], Oualid Rabia[1], Saber Saidi[1], Adel Taaboucheb[2], Badis Rahal[3], Lyes Benharrat[4], Hacene Serrar[5] and Moukhtar Boudissa[6]

[1]Laboratoire Technologie des Matériaux Avancés,Ecole Nationale Polytechnique de Constantine Malek BENNABI,BP 75A RP,Ali Mendjeli, 25000, Constantine, Algérie.

[2*]Laboratoire Couches Minces et Interfaces, Université de Fréres Mentouri Constantine 1, Constantine, 25000, Constantine, Algérie.

[3]Nuclear Techniques Division, Nuclear Research Center of Algiers, 2 Bd, Frantz Fanon, BP 399, 16000, Algiers, Algeria.

[4]Research Center in Semiconductors Technology for Energy-CRTSE, 02, Bd. Dr. Frantz Fanon, B.P. 140,7 Merveilles, 16038, Algiers, Algeria.

[5]Research Center in Industrial Technologies (CRTI), BP 64 Cheraga, Alger, Algeria.

[6]ENMC Laboratory, Department of Physics, Faculty of Science, University Ferhat Abbas, Setif, 19000, Algeria.

*Corresponding author(s). E-mail(s): abdelouadoud.mammeri@gmail.com;
Contributing authors: ybouachiba@gmail.com; a_bouabellou@yahoo.fr; oualidrabia28@gmail.com; saber18saidi@gmail.com; adelphm@gmail.com; b.rahal@crna.dz; benharrat.lyes@crtse.dz; serrarhacene@gmail.com; mokhtar.bousissa@univ-setif.dz;

1 Introduction

Zinc Oxide (ZnO) is is a multipurpose semiconductor with many uses such as ultra-capacitor electrode [**?**], spintronic devices [**?**], multigas sensing [**? ? ? ?**], piezoelectric devices [**?**], ultra-violet LEDs [**?**], detectors [**?**] as well as waveguides [**? ? ?**]. In its thin film form, ZnO has a large adaptation to several deposition methods such as chemical vapor deposition [**?**], pulsed laser deposition [**?**], spray pyrolysis [**?**], dip-coating [**?**] and electrochemical deposition [**?**]. ZnO has very interesting characteristics for application in electronics and optoelectronics devices, especially its exciton binding energy of 60 meV at 300K, a wide direct band gap of 3.37 eV [**?**]. In addition to an ordinary and extraordinary refractive indexes of $n_e = 2.006$ and $n_o = 1.990$ respectively [**?**]. To modify its electrical properties, ZnO was doped with Group III elements such as Al, Ga, and In who acted as donor dopants to reinforce its n-type electrical nature, and group V elements such as N, P, As and Sb who acted as acceptor dopants which changed ZnO to be a p-type semiconductor [**?**]. Controlling the refractive index of ZnO thin films was achieved by several ways including thermal annealing [**?**] and doping with In [**?**], Te, N [**?**] and Mg [**?**]. However, the effect of dopants on the optical and electrical properties of ZnO is still not well understood.

Tailoring ZnO optical and electrical properties via dopants while maintaining high quality films especially using spray pyrolysis is very attractive to both scientists and technology developers as it offers a control over several experimental parameters, it is cheap, uncomplicated and environmentally friendly.

Wurtzite $Mg_xZn_{1-x}O$ alloy is very interesting due to the high solubility of Mg in the ZnO wurtzite matrix (up to 30%) [**?**]. Moreover, it offers control over a range of optical and electrical properties of ZnO such as widening of the optical gap energy up to 0.85 eV [**?**], consequently, it can be used for multiple purposes such as a top layer in $Mg_xZn_{1-x}O$/ZnO multilayer UV photodetector [**?**] and high mobility MgZnO/ZnO thin film transistor [**?**] to name few. Concerning the waveguiding properties, little attention has been paid to wurtzite MgZnO as a waveguide, however, MgZnO was used as a buffer layer for ZnO waveguide thin film [**?**]. In an other work, a potential use of MgZnO cubic rocksalt-type phase as a wave guide was reported Yu et al. [**?**]. Wurtzite $Mg_xZn_{1-x}O$ thin film alloy refractive index was previously studied but there is still work to be done, as there are opposite results regarding the birefringence which is found to be negative in some studies [**? ?**] and positive in another study[**?**].

In this work, we engaged in the investigation of the relations between the refractive index, the gap energy and the charge carriers' density in addition to the birefringence of $Mg_xZn_{1-x}O$ thin films deposited by spray pyrolysis on glass substrate.

2 Results and Discussion

2.1 XRD analysis

From Figure **??**a we can see clearly that all films exhibit a crystalline hexagonal wurtzite structure (JCPDS card no. 00-036-1451) with the quasi-predominant of (002) peak indicating the preferential growth of undoped and Mg doped ZnO thin films through the c-axis direction. However, weak intensity peaks of other crystalline directions were observed in the following positions 31.96°(100), 36.56°(101), 47.87°(102), 63.17°(103) and 72.85°(004). The peak (002) experienced a shift towards higher angles (Figure **??**b) over Mg doping which was reported by a number of authors [**?** **?** **?**], and it is due to the difference in the ionic radius between Mg^{+2} (0.57 Å) and Zn^{+2} (0.60 Å) [**?**]. This difference is directly related to the compression strain on the main axes of the wurtzite structure a and c. Previously, Chang et al. [**?**] reported also similar compression strain in their sputtered MgZnO thin films which were interpreted by good substitution between Mg and Zn ions.
The grain size can be calculated by Debye-Scherrer formula [**?**]:

$$D = \frac{K\lambda}{\beta \cos(\theta)} \tag{1}$$

where λ is the wavelength of the incident X-ray, θ is the Bragg's angle, K is the shape factor (0.9 for gaussian fit), and β is the Full Width at Half Maxima (FWHM) of the peaks. The crystallite size, lattice parameters, and strain axes are tabulated in table 1. It should be noted that there was no significant change in the average crystallite size (33.13 nm for Mg_0Zn_1O film and an average of 33.03 nm for the $Mg_xZn_{1-x}O$ films), and the minus sign of the strain values (ϵ_a and ϵ_c) approves the compression nature of the strain. To calculate lattice parameter c of the thin films we used the Bragg's law (with n=1) and the d spacing of wurtzite structure.

2.2 UV-Vis measurements

The transmittance of the thin films was slightly enhanced on average with the introduction of Mg in the visible region (400-800 nm).The limit of the absorption zone was shifted to smaller wavelengths which renders the thin films to be more dielectric as Mg doping is increased, this effect is directly related to the blue shift of the band gap and it was approximated for each film using the Tauc's plot:

$$\alpha h\nu = A(h\nu - E_g)^n \tag{2}$$

where $h\nu$ is the photon energy, E_g is the gap energy, A is constant, and n equals $\frac{1}{2}$ since ZnO has a direct band gap. The widening of the optical band gap could be ascribed to the difference in electronegativity between Zn^{+2} and Mg^{+2} ions [**?** **?** **?**]. In similar study, Al-Ghamdi [**?**] reported this correlation between the optical band gap energy and the electronegativity in his work about amorphous $Se_{96-x}Te_4Ag_x$ thin films.

In fact, it should be noted that both the electronegativity and electron affinity are directly related [**?**]. In this way Figure 4 presents the calculated optical band gap and the electron affinity versus Mg doping. The electron affinity ($e\chi$) was quantitatively calculated using Vegard's law [**?**]:

$$e\chi(Mg_xZn_{1-x}O) = e\chi(ZnO) - (e\chi(ZnO) - e\chi(MgO))x \tag{3}$$

$e\chi(ZnO)$, $e\chi(MgO)$ have the value of 4.5 eV [**?**] and 0.85 eV [**?**] for the electron affinity of ZnO and MgO respectively. Previously, iskenderoglu et al. [**?**] approved experimentally by UPS technique the inverse relation between the gap energy and the electron affinity of sprayed MgZnO alloy thin film, with Mg doping ranging from 0 to 15%.

2.3 Photoluminescence

The room temperature photoluminescence spectra were shown in Figure 5 The undoped thin film had four peaks at 381 (3.25 eV), 416 (2.98 eV), 441 (2.81 eV) and 505 nm (2.46 eV) which were explained by: the emission corresponding to gap recombination, zinc interstitial (Zn_i), oxygen vacancies (V_O) and donor V_O – acceptor V_{Zn} recombination respectively [**?** **?**]. The same peaks were observed also in $Mg_{0.01}Zn_{0.99}O$ except a blue shift of the 380 peak to 381 nm (3.26 eV). The $Mg_{0.03}Zn_{0.97}O$ thin film had three peaks 379 (3.27 eV), 416 (2.81 eV), and 492 nm (2.52 eV) and they were attributed to gap recombination, zinc interstitial (Zn_i) [**?**] and oxygen vacancy (V_O) [**?**] respectively. Finally the $Mg_{0.05}Zn_{0.95}O$ thin film exhibited two peaks at 378 (3.28 eV) and 503 nm (2.47 eV) and they were manifestations of gap and donor V_O – acceptor V_{Zn} recombinations [**?** **?**]. The blue shift of the near band edge emission from the PL peaks was in consistency with the UV visible calculations of the optical band gap, however, it was at a lower rate which was explained by stokes shift [**?**].

2.4 Electrical measurements

Figure 6 demonstrates the near isotropic electric transportation of the deposited films which could be attributed to the fact that the films have the predominant orientation (002) of the wurtzite structure [**?**].
The free charge carriers density decreases from 3.146×10^{18} for the undoped film to 9.273×10^{13} cm^{-3} for $Mg_{0.05}Zn_{0.95}O$ film. In parallel, the resistivity increased from 109 to 1268 Ω cm and the mobility increases from 0.01821 to 53.08 $cm^2/(V.s)$. The decreased charge carriers' density could be attributed to the fact that the conduction band (CB) of pure ZnO consists mainly of O_{2p} and Zn_{4s} states [**?** **?**], so the introduction of Mg in ZnO thin films will reduce the Zn_{4s} state and introduce Mg_{3p} state which has high energy relative to the Zn_{4s} [**?** **?**]. Moreover, the widening in the optical bang gap energy discussed previously, could also influence the free charge carriers' density since the electrons passing from the valance band must have higher energy to access the conduction band.

2.5 Surface morphology

Figure 8 shows the morphology of undoped and 5 at. % doped ZnO thin films. The undoped (Figure 8a) thin film shows an inhomogeneous and dense structure with granular mixture of small grains and large aggregates. The size of the small grains varies from $\sim$ 20 to 80 nm and that of the aggregates reaches $\sim$ 200-300 nm. Suggesting the doped sample (Figure 8b), it is evident that magnesium has a tendency to promote the phenomenon of coalescence. This doped film shows a less dense and relatively homogeneous morphology with large aggregates whose size varies from $\sim$ 200 to 500 nm.
No cracks nor empty holes were observed on the surface of the films, revealing the high quality of our films.

2.6 M-lines measurements

The M-lines measurements demonstrate the guiding modes present in the films. All films have four guiding modes (TE_0, TE_1, TM_0, and TM_1) two for each optical polarization (Transverse Electric mode (TE) and Transverse Magnetic mode (TM)) as illustrated in Figure 9. Using the dispersion equations for TE and TM polarizations, the optogeometric parameters can be calculated [**?** **?** **?**]. The effective indices, the films thicknesses, and the birefringence values are presented in Table 2.
Figure 10 illustrate the variation of n_{TE}, n_{TM}, optical gap energy and free charge carriers' density as a function of the Mg concentration. The slight difference between n_{TE} and n_{TM} confirms the birefringence behavior of our films. This makes the guided waves traveling during the TE mode in the plane perpendicular to the *c*-axis of the wurtzite structure submit to an ordinary refractive index (n_{TE}) and during the TM mode to an extraordinary one (n_{TM}) [**?**]. Both n_{TE} and n_{TM} were found to decreased over Mg doping. This behavior seems to be in good agreement with the broadening of the optical band gap and the depletion of the conduction band free charge carriers' (Figure 10) [**?**]. The birefringence was measure to be positive for all films which is a good indication for the unchanging orientation of the bond with the replacement of Zn^{+2} by Mg^{+2} [**?** **?**].
The inverse relation between the optical gap energy, the resistivity and the refractive index as Mg content increased in the ZnO thin film was also observed by Kaushal et al. [**?**]. The same fact has been reported by Teng et al. [**?**] for Mg-doped ZnO thin films prepared by pulsed laser deposition. In similar study, Sorar et al. [**?**] found that the ordinary refractive index generally decreases with the increase of the Si doping in ZnO thin films prepared by sol-gel and annealed at 350 °C and 550 °C whereas their optical band gap energy was found to be blue shifted.

Table 1 The information obtained and calculated from the XRD spectra.

Sample	2θ (degree)	d spacing (Å)	Crystallite size (nm)	a(Å)	c(Å)	ϵ_a (10^{-3})	ϵ_c (10^{-3})
$Mg_{0.00}Zn_{1.00}O$	34.75	2.580	33.13	3.2306	5.1592	-3.4241	-5.4746
$Mg_{0.01}Zn_{0.99}O$	34.77	2.455	31.26	3.2240	5.1560	-5.4601	-6.0915
$Mg_{0.03}Zn_{0.97}O$	34.77	2.456	31.30	3.2256	5.1560	-4.9665	-6.0915
$Mg_{0.05}Zn_{0.95}O$	34.78	2.577	35.83	3.2298	5.1547	-3.6709	-6.3421

Table 2 Optogeometric Properties of the deposited thin films.

Sample	Effective index $\pm 10^{-4}$				Refractive index 10^{-4}		Thickness TE	Thickness TM	Birefringence
	TE_0	TE_1	TM_0	TM_1	n_{TE}	n_{TM}	$\pm 0.1nm$	$\pm 0.1nm$	$(n_{TM} - n_{TE})$
$Mg_{0.00}Zn_1.00O$	1.8923	1.6565	1.8793	1.6033	1.9699	1.9761	436.1	452.1	0.0062
$Mg_{0.01}Zn_{0.99}O$	1.8758	1.5994	1.8539	1.5486	1.9680	1.9682	347.4	382.6	0.0002
$Mg_{0.03}Zn_{0.97}O$	1.8738	1.6203	1.8581	1.5647	1.9580	1.9652	413.1	426.3	0.0072
$Mg_{0.05}Zn_{0.95}O$	1.8451	1.5981	1.8278	1.5494	1.9278	1.9314	417.7	433.7	0.0036

3 Tables

4 Figures

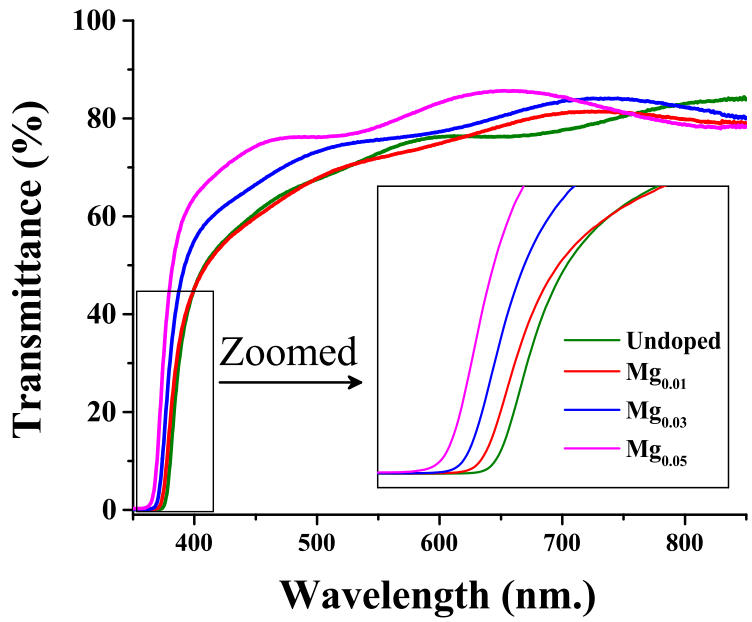

Fig. 2 Transmittance spectra of pure and doped ZnO thin films zoomed in the absorption region.

5 Methods

The sprayed solution for the undoped ZnO thin films was prepared by dissolving the proper amount of dihydrate zinc acetate [$Zn(CH_3CO_2)_2 \cdot 2H_2O$] in 99.98% pure methanol to obtain 0.1 M solution that was submitted to a constant stirring at 60 °C for 45 min on a magnetic stirrer. Concerning the sprayed solution of the Mg doped ZnO thin films, we maintained the same parameters with the use of magnesium chloride [$Mg(CH_3CO_2)_2 \cdot 4H_2O$] as Mg precursor, and each time the proper amount was added to 0.1 M methanol solutions of $Zn(CH_3CO_2)_2 \cdot 2H_2O$ to produce the following contents of zinc and magnesium: $Mg_xZn_{1-x}O$ with x equals 0.01, 0.03 and 0.05.
An ordinary glass substrate were ultra-sonically cleaned in a 1:1 mixture of acetone and ethanol for 15 min and left to dry in air. The films were deposited using spray pyrolysis system. The deposition temperature was 450 °C.

In order to characterize our thin films, multiple techniques were used: Philips PANalytical X'Pert Pro diffractometer with a wave length of 1.5406 Å, environmental scanning electron microscope Philips XL30 ESEM FEG and for the electrical properties Ecopia HMS-3000 hall effect measurement system, finally for the optical measurements, Metricon 2010/M Prism (rutile TiO_2: n_e=2,8639 and n_o=2.5822 at 632,8 nm with an angle of A_p=44,60 °) Coupler was used to couple 632.8 nm HeNe laser light into air/$Mg_xZn_{1-x}O$/glass waveguide and Shimadzu UV-3101PC Spectrophotometer.

6 Conclusion

Mg doped ZnO thin films were successfully deposited on glass substrate via spray pyrolysis at 450 °C. The XRD characterization showed highly *c* oriented thin films with a decrease in *a* and *c* as the Mg concentration increased in the thin films. The undoped thin film had a multisize grain distribution meanwhile the $Mg_{0.05}Zn_{0.95}O$ had a more homogeneous grain distribution. Mg doping in the ZnO films led to a blue shift of the optical band gap energy and a depletion of the conduction band due to the drop in free carriers' density that had a direct effect on the ordinary and the extraordinary refractive indexes that were found to decrease. The birefringence of a crystal depends on multiple factors such as strain, defects charge carriers' density, bound orientation and so on, therefore it will change from papers to papers with the change of deposition method especially.

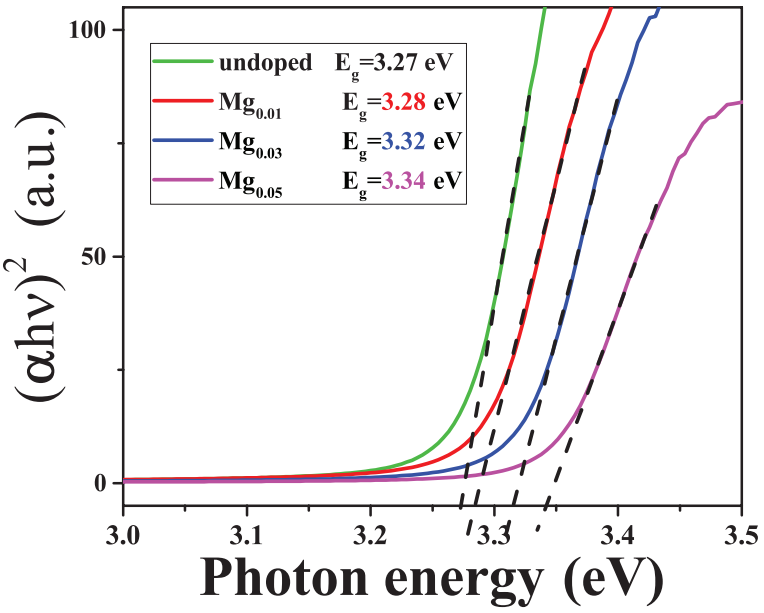

Fig. 3 Tauc's plot for the undoped and doped ZnO thin films.

Declarations

- Funding: Not applicable
- Conflict of interest/Competing interests: The authors declare that they have no conflict of interest.
- Ethics approval: Not applicable
- Consent to participate: Not applicable
- Consent for publication: Not applicable
- Availability of data and materials: Not applicable
- Code availability: Not applicable
- Authors' contributions: Not applicable

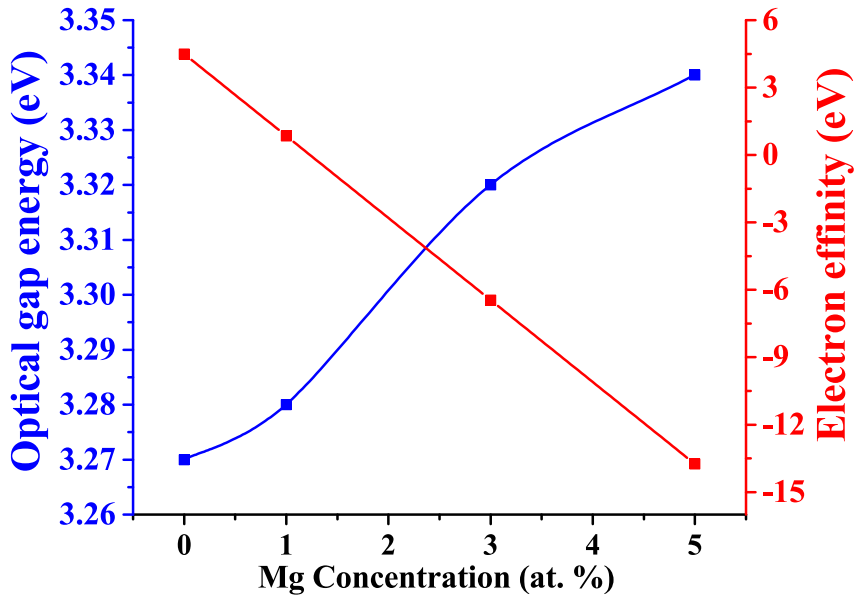

Fig. 4 The evolution of the optical band gap energy and the electron affinity of $Mg_xZn_{1-x}O$ thin films as a function of Mg concentration.

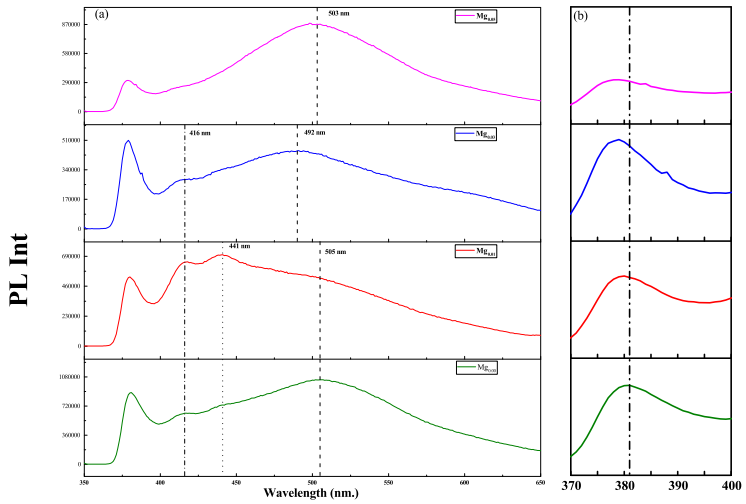

Fig. 5 (a) Room temperature photoluminescence spectra, (b) an emphasis of the excitons recombination peaks

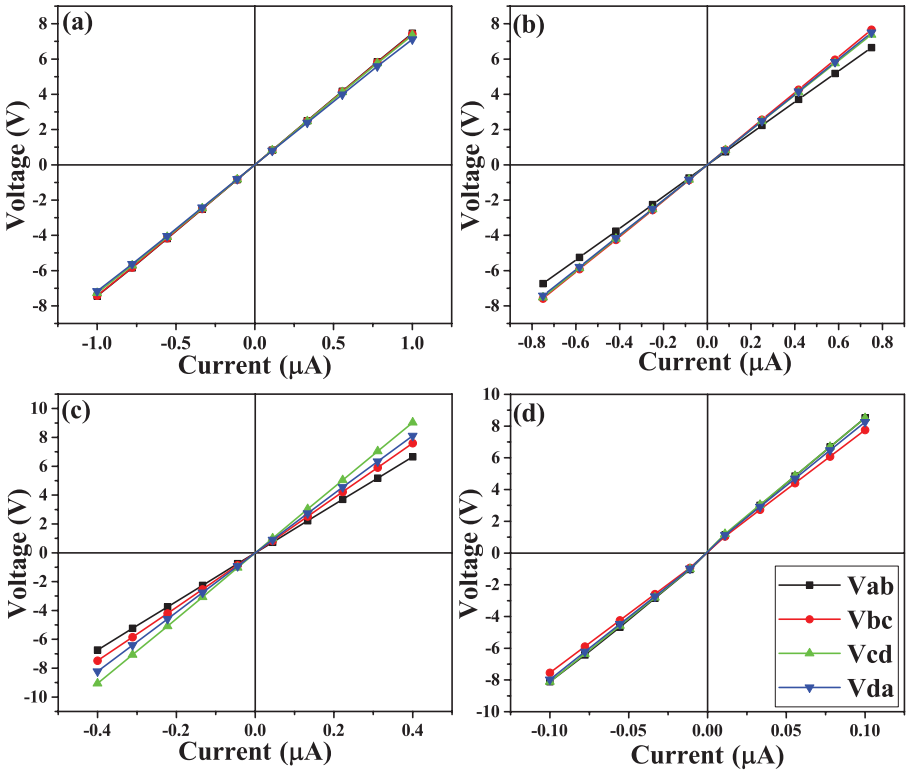

Fig. 6 I-V measurements for the four thin films: (a) undoped ZnO, (b) $Mg_{0.01}Zn_{0.99}O$, (c) $Mg_{0.03}Zn_{0.97}O$ and (d) $Mg_{0.05}Zn_{0.95}O$.